The Thesis Committee for Sandra Nkechinyere Ezidiegwu
Certifies that this is the approved version of the following thesis:

Investigation of the Pore Size and Structure in Organic-Rich Shales

APPROVED BY
SUPERVISING COMMITTEE:

Supervisor:

Hugh Daigle

David Nicolas Espinoza

Investigation of the Pore Size and Structure in Organic-Rich Shales

by

Sandra Nkechinyere Ezidiegwu, B.S.

Thesis

Presented to the Faculty of the Graduate School of

The University of Texas at Austin

in Partial Fulfillment

of the Requirements

for the Degree of

Master of Science in Engineering

The University of Texas at Austin

May 2015

Dedication

To my family and friends.

Acknowledgements

I would like to express my deep appreciation and gratitude to my supervisor, Dr. Hugh Daigle, for his guidance, support and constant encouragement in the completion of this work. I would also like to thank Frankie Hart for her guidance throughout my studies here at the University of Texas at Austin. I would also like to thank Glen J. Baum for his assistance on my research and laboratory work. Thank you to my colleagues on Dr. Daigle's team: Bishwas Ghimire and Chunbi Jiang, who made using a Porosimeter fun.

I would like to acknowledge the Bureau of Economic Geology (BEG) for their provision of the samples used, and Humble Geochemical Services for their aid in making this experiment a reality.

And finally, I would like to thank the Statoil Fellowship Program and the Statoil Steering team for their financial support because without them, this would not have been possible.

Abstract

Investigation of the Pore Size and Structure in Organic-Rich Shales

Sandra Nkechinyere Ezidiegwu, M.S.E

The University of Texas at Austin, 2015

Supervisor: Hugh Daigle

Permeability in source rocks allows the flow of reservoir fluids during production and is dependent on the pore size distribution. In organic shales, the level of porosity of organic material (OM) is based on its range of pore sizes. Scanning electron microscope (SEM) images are commonly used to examine OM-hosted pores, but this technique is limited by resolution, which is in the order of ~5 nm. This study seeks to increase this range of pore size distribution (PSD) to ~ 0.38 nm, in organic-rich shales by using low-pressure carbon dioxide (CO_2) adsorption coupled with density functional theory (DFT). In addition, we coupled low-pressure nitrogen (N_2) adsorption with the Barrett-Joyner-Halenda (BJH) and DFT models to quantify pore sizes between ~2 to 170 nm. To characterize the entire range of pore sizes, we used high-pressure mercury intrusion because it is commonly used to quantify larger pores.

The samples used in this study include a bulk sample and isolated kerogen of Green River shale (Eocene, Utah), Woodford shale (Upper Devonian, Oklahoma), and

Cameo Coal (Cretaceous, Colorado). These samples represent type I, II and III, kerogen, respectively, at similar maturity levels and thus provide a good experimental basis for evaluating the PSD. The methodology consisted of four steps: i) Kerogens were isolated from the bulk samples by demineralization, ii) Samples were divided into sizes of ~ 0.5 grams into test tubes and degassed, iii) Samples were analyzed in the Porosimeter using low-pressure N_2 and CO_2 adsorption techniques, iv) Isotherm data from the adsorption measurement were extracted to create the PSD.

Our results showed the presence of pore sizes as small as ~ 0.38 nm, based on combining techniques of N_2 adsorption at 77 K and CO_2 adsorption at 273 K in all three samples. Hence, we have expanded our understanding of the range of pore sizes contained in organic-rich material. In addition, the majority of pores in Green River shale and cameo coal fell below the SEM resolution limit of ~5 nm. Lastly, the kerogen and bulk samples of the Green River and Woodford shales showed a variation in the PSD, with the larger pores in the kerogen, which indicates that kerogen constitutes the majority of the pores in the samples. In conclusion, we developed a novel approach to investigate OM-hosted pore sizes. This approach increased the range of pore sizes from ~ 5 nm to ~ 0.38 nm, thus improving the estimation of flow rates during production in shale and in applicable reservoirs.

Table of Contents

List of Tables

List of Figures

CHAPTER 1: INTRODUCTION

Oil and gas in the US play a vital role in economic growth. With the increasing impact of unconventional hydrocarbons on the economy, it is necessary to better understand how to optimize these resources, specifically, shale in shale basins. Adsorption techniques are widely used to comprehensively characterize porous material with respect to the surface area, pore size distribution, and porosity (Thommes & Quantachrome Instruments 2003). If we can accurately quantify the porosity in organic-rich materials, we can determine the volume of pores that contain hydrocarbons, and ultimately make better predictions of production rates and reserves. In addition to quantifying porosity, generating petroleum in a source rock directly correlates to its volume, organic-richness, and thermal maturity. Organic richness refers to the organic content of the source rock, while thermal maturity refers to the amount of heat exposure a rock has undergone, which co-controls the hydrocarbon saturation level in the rock.

In this study, we investigated the pore size and structures of samples from the Green River shale formation of the Eocene age in Utah, the Woodford shale formation of the upper Devonian age in Oklahoma, and the Cameo Coal zone of the Cretaceous age in Colorado. These samples represent the main types of kerogen, types I, II and III, respectively. Type I kerogens are derived from lacustrine environments, type II kerogens are found in deep marine environments, and type III kerogens are derived from terrestrial plant debris (McCarthy et al. 2011). Experiments on shale samples from the Green River and Woodford formations were carried out separately on bulk shales and isolated kerogen

to investigate their pore size and the structure of their organic and non-organic content. To assess the influence of kerogen type and thermal maturity on adsorption in shales, Zhang et al. investigated the adsorption of methane onto whole rock and onto the isolated kerogen of the Green River Formation, Woodford Shale, and Cameo Coal. The total organic carbon (TOC) content of these samples was 20.7, 17.2, and 72.2%, respectively, with similar thermal maturities ranging from 0.56 to 0.58 % Ro. Their results indicated that larger amounts of gas can be adsorbed onto isolated kerogen than onto whole (Zhang et al. 2012). The desorption of gas from the surface of OM-hosted pores and the diffusion within the organic matter appear to be an important mechanism for moving hydrocarbon out of the rock (Shabro et al. 2012).

OM-hosted pores are commonly investigated using scanning electron microscope (SEM) images, which generally have a resolution on the order of ~ 5 nm (Chalmers et al. 2012). Comparisons between helium porosity and porosity determined from SEM images suggests that >50% of the porosity in organic shales may be contained in pores smaller than this limit of ~ 5 nm (Milliken et al. 2013). The adsorption of N_2 at 77 K is widely used to characterize micropores as small as 0.51 nm in natural and industrial porous media. Measurements of N_2 adsorption on shale samples have shown significant pore volumes in pores smaller than 2 nm in width (Adesida et al. 2011), which is below the resolution of SEM. This suggests that the missing porosity inferred by Milliken et al. is present in these micro-pores. Due to more favorable molecular kinetics, CO_2 can enter and assess pores as small as 0.35 nm (Chalmers et al. 2012), which should account for the

missing micropores. CO_2 adsorption can therefore extend the lower limit of micropore characterization.

This study combines N_2 and CO_2 adsorption techniques, enabling us to quantify pores from 0.3 nm to 200 nm in width. A pore size distribution is generated from data analysis of the adsorption isotherms produced by adsorption measurements. In order to manipulate the data points, several computational models can be used. Although, the Barrett-Joyner-Halenda (BJH) model is commonly used, it may lead to significant errors because it is based on the theory that pores are cylindrical and because the BJH model does not account for interactions between absorbed films on opposing walls of micropores (Lastoskie et al. 1993). According to Lastokie et al. the use of the density functional theory (DFT) model, assuming a slit-pore structure, yielded results that are more reliable than other analysis methods which do not correctly describe micro-pore filling (Lastoskie et al. 1993). Hence, in this paper, we use low-pressure gas adsorptions of carbon dioxide and nitrogen coupled with the DFT model, which assumes a slit pore structure to characterize the micro-porosity, specifically, the OM-hosted porosity, which previous investigations have failed to quantify.

In organic shales, the organic matter makes up the bulk of the porosity. The lack of understanding of the pore structure of these low-permeability rocks hinders an economical production of hydrocarbons (Lastoskie et al. 1993). Therefore, by determining the pore structure of these rocks we can develop a better assessment of shale basins and thus produce strategically.

1.1. THESIS OUTLINE

This thesis comprises of six chapters. The first chapter is an introduction into the impact of shale plays in the US and why an investigation into the pore size and structure is of importance. The second chapter covers the literature review behind the experiments run and previous research that has been carried out on pore structure of shales. The third chapter entails the materials, methods and procedures used in carrying out the experiments on the various samples. The fourth chapter contains an analysis of the data drawn from the experiment as well as a discussion on the results. Lastly, the fifth chapter states the conclusion drawn from the experiments and suggestions for further research.

CHAPTER 2: BACKGROUND AND LITERATURE REVIEW

2.1 ADSORPTION

Adsorption is a widely adopted technique used to characterize the pore sizes and structures in porous matter. This technique, however, requires an in-depth understanding of the fundamental processes associated with phase interactions and adsorption isotherms. Pore size distributions are obtained by manipulating the isotherm data and provide us with information on the pore sizes in porous matter.

2.1.1 Gas-Solid Interaction

Adsorption involves the interaction between two or more molecules. It can be a gas-solid interaction or a liquid-solid interaction. This paper focuses on the physical adsorption of a gas onto a solid surface. Desorption is the removal of the gas or liquid molecules from solid surfaces and is also the reverse of adsorption. Desorption is a technique that can also be used in the production of hydrocarbons from reservoirs.

In adsorption, the interaction energy displayed between the gas and solid particles controls the adsorption process. The isotherm shape is based on the solid-fluid interaction potential (Lastoskie et al. 1993). The solid-gas interaction potential in this study is expressed as the Lennard-Jones 12-6 expression (Steele 1973).

$$\ell_{gs}(r_{i,j}) = 4e_{gs}\left\{\left(\frac{s_{gs}}{r_{i,j}}\right)^{12} - \left(\frac{s_{gs}}{r_{i,j}}\right)^{6}\right\}$$

where $\ell_{gs}(r_{i,j})$ is the interaction of the ith gas atom and the jth substrate atom or molecule (in this study: the interaction of the N_2 or CO_2 atom with the samples), e_{gs} is the depth of the inter-molecular potential well, s_{gs} is the molecular diameter, and $r_{i,j}$ is the internuclear separation of the molecules (Ryu et al. 1999). Table 2.2 below shows the interaction parameters assumed in this study computed by the Micrometrics 3Flex system based on the adsorbent and adsorbate properties shown in Table 2.1.

		Adsorbent	Adsorbate	
			CO_2	N_2
Diameter	(Å)	2.76	3.23	3
Diameter @ Zero Energy	(Å)	2.369	2.77	2.574
Polarizability	(cm^3)	2.50E-24	2.70E-24	1.76E-24
Magnetic Susceptibility	(cm^3)	1.30E-29	5.00E-29	3.60E-29
Density	(mol/cm^3)	1.31E+15	5.45E+14	6.71E+14

Table 2.1: Adsorbent and adsorbate properties.

Interaction Parameters				
			CO_2	N_2
Woodford Shale	Kerogen	($erg.cm^4$)	2.67E-43	1.70E-43
	Bulk Shale		2.67E-43	1.70E-43
Green River Shale	Kerogen		2.67E-43	1.70E-43
	Bulk Shale		2.67E-43	1.70E-43
Cameo Coal			2.67E-43	1.70E-43

Table 2.2: Interaction parameters between samples and respective adsorbate gases.

2.1.1.1 Density Functional Theory

The density functional theory (DFT) model is an effective tool used in characterizing porous material. This approach uses statistical thermodynamics to construct model isotherms that account for gas-solid and gas-gas interactions along with the geometric configurations of the pore walls during adsorption. In this study, the pore geometry is assumed to have slit-pore geometry. According to this theory, pore filling is controlled by the solid-gas and gas-gas interactions which may take the form of micro pore filling or capillary condensation (Sing 2001). The pore size distribution was calculated using the density functional theory software on the 3flex Micrometrics system.

2.1.2 Isotherm Supporting Theory

Isotherm graphs describe the equilibrium relationship between the amounts of adsorbate adsorbed on the adsorbent surface during adsorption. These graphs are expressed as a function of equilibrium concentration. In this study, the isotherm graphs were evaluated based on two isotherm equations namely, Langmuir and Freundlich.

2.1.2.1 Langmuir and Freundlich Isotherms

Langmuir adsorption isotherms depend on the assumption that an intermolecular force decrease rapidly with distance and as a result, predicts the existence of monolayer coverage of the adsorbate on the outer surface of the adsorbent. The Langmuir equation assumes a structurally homogenous adsorbent where all adsorption sites are identical and

energetically equivalent. The adsorption capacity of the adsorbent can be represented by the expression below (Wong et al. 2004).

$$q_e = \frac{q_m K_L C_e}{1 + K_L C_e}$$

where q_e is the adsorption capacity of the adsorbent at equilibrium (mmol/g), q_m is the maximal adsorption capacity, C_e is the adsorbate concentration at equilibrium (mmol/L), and K_L is a Langmuir isotherm constant related to free energy of the adsorption (Liu et al. 2010).

Freundlich model is an empirical equation that assumes heterogeneous adsorptive energies on the surface of the adsorbent (Liu et al. 2010), and is characterized by the heterogeneity factor of 1/n (Wong et al. 2004). This empirical equation can be expressed as shown below.

$$q_e = K_F C_e^{1/n}$$

where q_e is the adsorption capacity of the adsorbent at equlibirum (mmol/g), C_e is the adsorbate concentration at equilibrium (mmol/L), and K_F and n are Freundlich constants related to the adsorption capacity and adsorption intensity, respectively (Liu et al. 2010). A linear form of the Freundlich equation can be obtained by taking logarithms of the equation shown above to produce that which is displayed below.

$$\ln q_e = \ln K_F + \frac{1}{n} \ln C_e$$

From this derivation, a plot of $\ln q_e$ versus $\ln C_e$ will enable the determination of the constant K_F and exponent $1/n$. The Freundlich isotherm also describes reversible adsorption and is not restricted to monolayer adsorption (Wong et al. 2004).

2.1.3 Pore Filling

The process by which the pores are filled during adsorption is reflected in the isotherm graphs. In adsorption, there is either a monolayer adsorption of the gas (adsorbate) onto the solid (adsorbent) or a multilayer adsorption. Typically, micro-pores are associated with Type I isotherms, which display a monolayer adsorption, while mesoporous and macroporous solids show a hysteresis loop that is characteristic of Type IV isotherm.

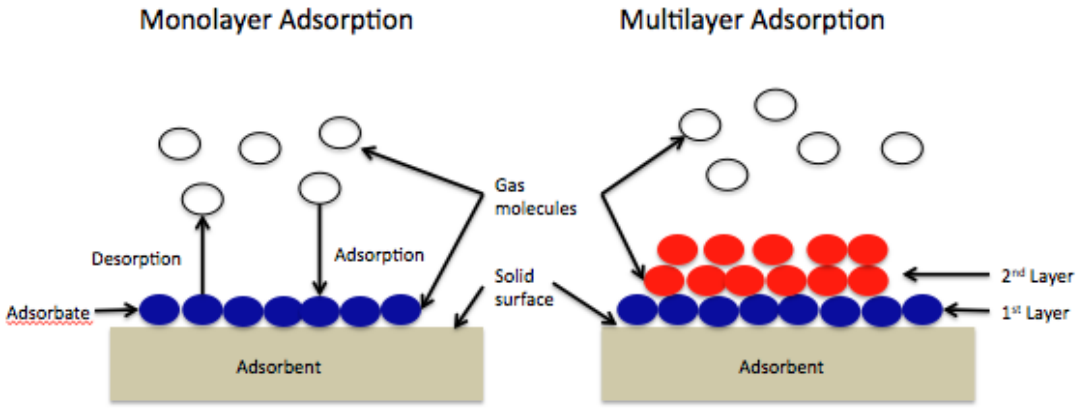

Figure 2.1: Presentation of a typical adsorption process.

2.1.3.1 Isotherms and Hysteresis Loops

Shown below in Figure 2.2 are the six main isotherms attributed to physical adsorption. The various types of isotherms provide information on the process by which pores were filled and the types of pores located in the solid matter.

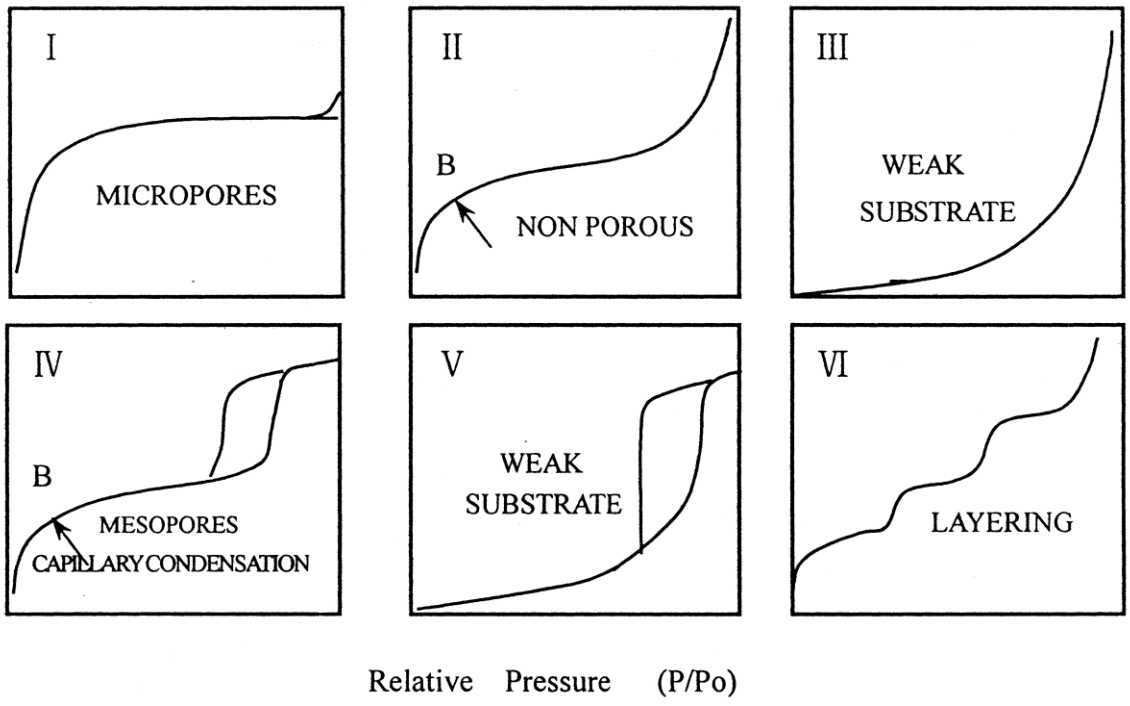

Figure 2.2: IUPAC classification of adsorption isotherms (Ryu et al. 1999).

Ryu et al. in his paper "*Characterization of pore size distributions of carbonaceous adsorbents by DFT"* defined the six isotherm types shown above in Figure 2.2, which were classified according to the process of adsorption that took place and on the pore structure of the adsorbents.

> "The Type I isotherm is given by microporous solids and is concave to the P/Po axis and adsorption amount approaches a limiting value as P/Po $\rightarrow$ 1. The very steep region at low P/Po is due to the filling of very narrow pores and limiting uptake is dependent on the accessible micropore volume rather than on the internal surface area. The Type II isotherm is normally given by a nonporous or macroporous adsorbent on which unrestricted monolayer–multilayer adsorption can occur. The appearance of point B indicates the stage where monolayer coverage is completed and multilayer adsorption begins. The Type III isotherm is generally associated with weak adsorbent–adsorbate and relatively strong adsorbate–adsorbate interactions. In this case cooperative effects lead to the development of patches of multilayer before a uniform monolayer has been formed" (Ryu et al. 1999).

Hysteresis loops are commonly displayed in the multilayer range of physical adsorption and are associated with the filling and emptying of mesopores (Sing 2001). Hysteresis loops are also characteristic of Type IV isotherms. The similarities between the initial parts of Types II and IV isotherms show that a monolayer adsorption was followed by a multilayer adsorption, which then contributed to the hysteresis loop. The Type V isotherm, which is similar to Type III, represents a weak adsorbent-adsorbate interaction. Type VI isotherm represents a stepwise multilayer adsorption on a uniform non-porous surface. Each step height provides a measure of the capacity for each adsorbed layer (Ryu et al. 1999). We observed the presence of Type I isotherms from the adsorption of CO_2

and Type IV isotherms from the adsorption of N_2. These isotherm graphs are shown in Figures 4.1 – 4.5.

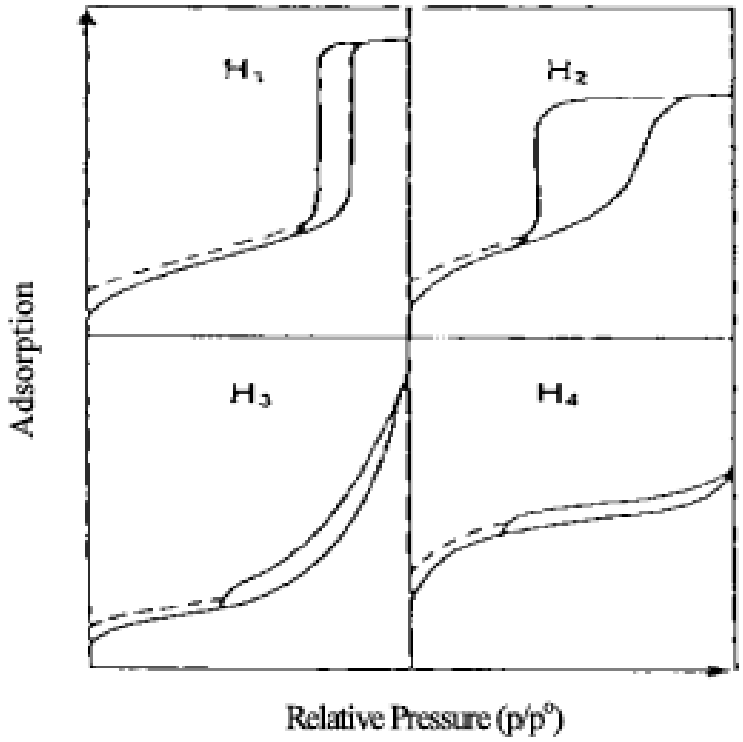

Figure 2.3: The modern classification of hysteresis loops (Sangwichien et al. 2002).

The shapes of hysteresis loops are important because they provide information on the pore size distribution and structure of the solid. Shown above in Figure 2.3 is a graph that describes four different types of hysteresis loops. Type H-1 has a narrow hysteresis loop with almost vertical and parallel adsorption and desorption curves. This type of graph signifies that the adsorbent is associated with porous materials made from agglomerates of approximately uniform spheres and has a limited pore-size distribution. Type H-2 is

associated with porous adsorbents that have a broad distribution of pore sizes and shapes. Type H-3 shows no limiting adsorption at high relative pressures and is attributed to porous adsorbents with plate-like properties which gives rise to sit shaped pores. Type H-4 is equally associated with narrow slit-like pores (Sangwichien et al. 2002). In this study, the isotherm graphs of all three samples showed no limiting adsorption at high relative pressures and contained hysteresis loops that signify the presence of slit-like pores.

CHAPTER 3: MATERIALS AND METHODS

3.1 MATERIALS, METHODS AND PROCEDURES

This chapter covers the materials and methods used in carrying out adsorption measurements. The term adsorption refers to the physical or chemical interaction between two matters. In this study, adsorption represents the physical attraction of the gas matter, the absorbate, unto the surface of the solid matter, the absorbent. This allows the gas matter to fill up the pore spaces contained in the rock samples and hence, produce an adequate quantification of the rock porosity by using a Porosimeter. This study used 3 samples, namely: Green River Shale, Woodford shale, and Cameo Coal, which were obtained from Utah, Wyoming, and Colorado, respectively and provided by the Bureau of Economic Geology (BEG). To accurately quantify the pore sizes, the Green River and Woodford shale kerogens were isolated from the bulk shales using a technique known as demineralization by Humble Geotechnical Services. Once each adsorption measurement had been completed, an analysis on the adsorption isotherms determined the pore size distribution.

3.1.1 Sample Preparation and Materials Used

Each sample was taken from their respective cores and divided into two aliquots of ~ 1g for nitrogen and carbon dioxide adsorption measurements. Using the mortar and pestle in Figure 1 below, each sample was ground to produce finer particles to provide a larger surface area for the adsorption measurements. Approximately 0.5g of each sample

was then placed into a long neck test tube following the grinding and weighed on the scale shown below.

Figure 3.1: Mortar, pestle and scale used in preparing samples.

3.1.1.1. Degasser

In this study, we used a SmartPrep degasser as described below to ensure all samples were free of any volatiles.

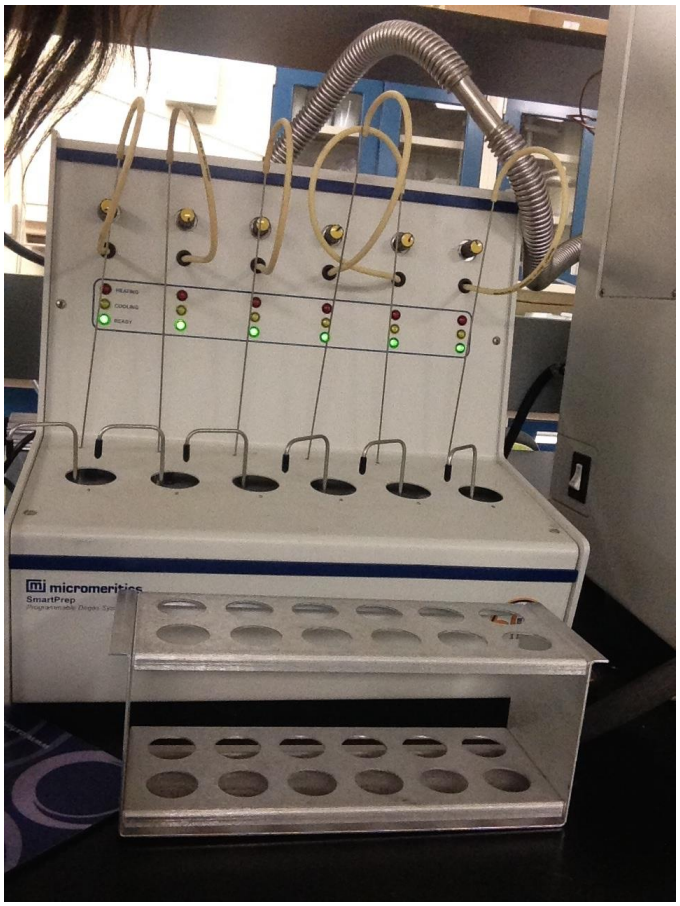

Figure 3.2: 6-port SmartPrep Degasser.

"The SmartPrep™ is a flowing-gas degassing unit which removes adsorbed contaminants from the surface and pores of your sample in preparation for analysis. It contains six sample ports, each one independently temperature-controlled for greater flexibility. It contains two serial ports, one for connecting to the computer and the other available for connection of an additional SmartPrep. The temperature, ramp rates, and soak times of each sample are individually

controlled by computer. Up to five ramps and soaks are allowed. All degas information is integrated into the sample data file for easy reference in the future." (Micromeritics.com, 2015)

3.1.1.2. Micrometrics 3Flex System

The adsorption measurements were conducted using a Micrometrics 3Flex system, Figure 3, and is described below.

Figure 3.3: Micrometrics Porosimeter used in running adsorption measurements.

"Micromeritics 3Flex Surface Characterization Analyzer is a fully automated, three-station instrument capable of high-performance physisorption (mesopore and micropore) and chemisorption analyses with superior accuracy, resolution, and data reduction. Each analysis station is upgradeable from mesopore to micropore with the option of designating one station for chemisorption analyses. All analysis stations can be configured for krypton analysis of low surface area materials. Vapor sorption capability is standard. A single 3Flex with its minimal footprint and three configurable analysis stations eliminates costly investment in multiple instruments and additional bench space. The 3Flex is ideally suited for the characterization of MOFs, zeolites, activated carbons, adsorbents, and a wide variety of porous and non-porous materials." (Micromeritics.com, 2015)

3.1.1.3. Gases and Pressure Gauges

In conducting this study, the following gases were used;

1. Nitrogen
2. Carbon Dioxide
3. Helium

It is important to ensure pressure gauges were properly calibrated and set at the right pressure.

3.1.2 Adsorption Experimental Procedure

1. Creating the Sample file

    a. Open Micrometrics 3Flex System software -> File -> New Sample

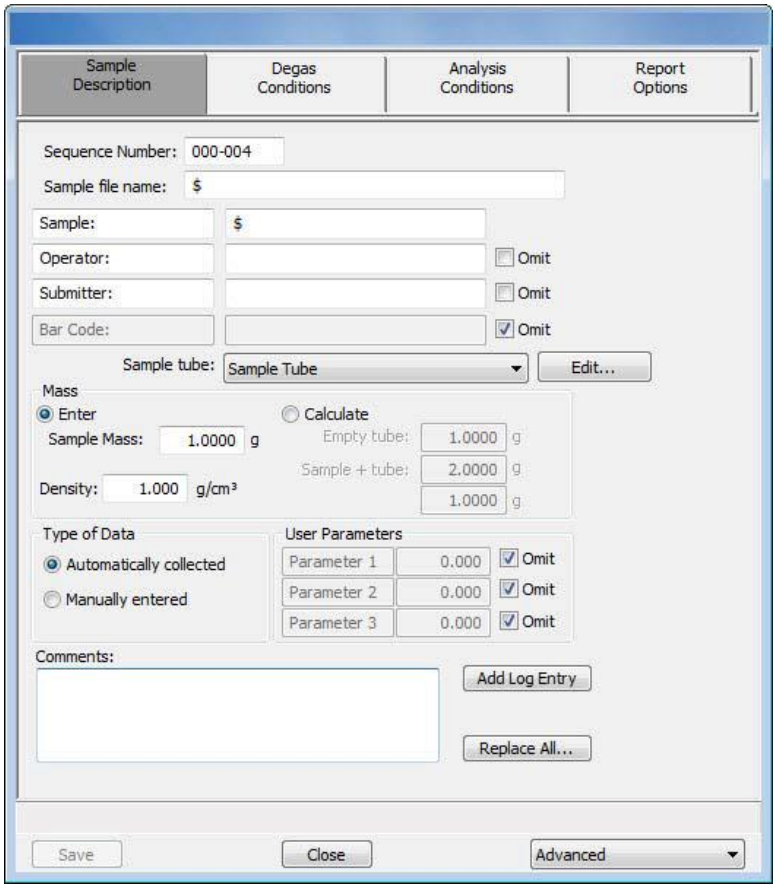

Figure 3.4: Pictorial diagram of window for imputing analysis conditions.

    b. In the **Sample Description** window as shown in Figure 4 above, data was input using the following steps:

        i. Method: Nitrogen Reference Material Silica Alumina

ii. Sample: From sample label (Expedition- Core- Section)

iii. Operator: SE

iv. Submitter: Based on company responsible for obtaining the sample

v. Sample tube: Default or tube name

vi. Calculate: Enter the weighed masses

vii. Density: Default (1.000 g/cc)

viii. Data: Automatically collected

ix. Comments: If any. Ideally, this text box was used to note degassing conditions and mass prior to running adsorption measurements.

c. In the **Degas Condition** window indicate the following;

i. Temperature: 100 ℃

ii. Rate: 10 ℃ / min

iii. Time: 240 min

d. In the **Analysis Condition** window, the following inputs were made;

i. Run Condition: Silica Alumina Nitrogen @ 77.35 K or Carbon Dioxide @ 273.15 K

ii. Adsorptive: Input the gas being used for adsorption from the drop down menu. N_2 or CO_2

iii. Preparation: Leak Test (Should work after degassing properly; if not, abort)

iv. Free Space: Default (measure before analysis)

v. P_0 Options: Default (measure in the tube for each isotherm point)

vi. Analysis Temperature: Default (calculate from P_0)

vii. Dosing Options: Default

viii. Termination: Default

e. In the **Report Options**, window the following were selected;

i. Silica Alumina Reference Material

ii. Show report title

iii. Show graphic

iv. Selected Reports: Select as needed

f. Lastly, save as a new sample file. Ensure that the sample label information is saved in the same format.

2. Degassing the sample

a. Weigh the empty sample tube first with stopper. Note the tube number.

b. Put some sample in the tube.

c. Weigh it just in case (perhaps, to compare), but weigh later after degassing too as that's the actual weight to be used.

d. Wipe the gas delivery tube and insert it into the tube. Lower it to right above the bulb, but do not touch the sample to avoid clogging in the tube.
e. Set stopper at the top loose enough to let the gas flow out and yet prevent unwanted contamination.
f. Insert the tube into one of the ports in the degas station and degas.
g. To degas, go to Unit1 -> Degas. Browse the saved sample file into appropriate port and start.
h. Open the valve on the SmartPrep degasser one fourth of a turn.

Once degassing has been completed, close the valve and remove the gas delivery tube slowly from the port. Press the stopper immediately to seal against contamination and weight the tube with sample and update the sample file with new weight value.

3. Installing sample tube

   To install the sample tubes unto the 3flex system, we followed the steps shown below.

   a. Remove the port plug (use port 2) by unscrewing the nut. Make sure the ring comes out too.
   b. Remove the stopper, and insert the filler rod. Hold the tube horizontally while doing this.
   c. Slide the isothermal jacket down over the tube until it touches the bulb.

d. Position the Dewar lid correctly to have the slot for Psat tube in the right position (match the numbers marked on it to the ports).
e. Insert the tube through the right hole, place the nut and ring, and screw the nut securely.
f. Insert the Psat tube into the slot.

Check that all valves have been properly tightened to avoid leaks in the Dewar. To prevent the risk of breaking test tubes, do not over-tighten the screws that connect the test tubes to the Dewar.

4. Preparing Dewar
    a. For nitrogen adsorptions, pour liquid N2 into the Dewar (for now, place Dewar on the floor while doing this). Don't fill to the top. Use the level indicator; don't let the liquid go beyond the indicator mark.

       For carbon dioxide adsorptions, pour ice cubes into the Dewar, followed by cold water. Using a thermometer, ensure that the temperature reads 0^{o}C. Make sure the mixture doesn't go beyond the indicator mark.
    b. Place Dewar on the elevator. Place Dewar lid ¾ of an inch below the nut, so that sealing on the top of Dewar is ensured.

5. Starting sample analysis

Ensure that all gas cylinders are filled with the correct gases and that the pressure gauges are correctly set.

a. Go to Unit1 -> Sample Analysis. Browse the appropriate sample file.
b. Check to see if some of the fields are populated.
c. START the analysis.

All necessary tests will be done automatically. Check back in half an hour to see if leak test has passed or not. If it passes the leak test, the test will continue normally. But in the event of a leak test failure, abort it, and proceed with the adsorption analysis.

CHAPTER 4: EXPERIMENTAL RESULTS AND DISCUSSION

4.1. GAS ADSORPTION

This section describes the results obtained from running gas adsorption measurements on three samples using a Micrometrics 3Flex system. This study combines nitrogen (N_2) and carbon dioxide (CO_2) adsorption techniques, enabling us to quantify pores from 0.3 nm to 200 nm in width. The samples used in this study include (1) The kerogen and bulk shale of Green River shale, (2) the kerogen and bulk shale of Woodford shale, and (3) Cameo Coal. These results will identify the adsorption capacities collected from the isotherm data, and the pore sizes of these samples.

4.1.1. Adsorption Measurement

In preparation, following the demineralization of the Green River and Woodford shale into kerogen and bulk shale, all three samples were crushed, weighed and degassed to ensure they were saturation free. During measurement, depending on the gas adsorption being run, CO_2 or N_2 is intruded into the samples using the Micrometrics 3flex system. Using the density functional theory and assuming slit-pores, the isotherm data collected from the adsorption measurement was translated into a pore size distribution. The pore size distribution graphs in Figures 4.9, 4.10, and 4.11, confirm the benefits of using CO_2 in identifying micro-pores in organic matter (OM) hosted pores, which also confirms Milliken's suggestion that over 50% of the porosity in organic shales may be

contained in pores smaller than the scanning electron microscope (SEM) image resolution limit of ~ 5 nm (Milliken et al. 2013).

4.1.1.1. Isotherm Data and Adsorption Capacities

The isotherm data describes the adsorption capacities of each sample with changes in relative pressure. As the samples are dosed with either N_2 or CO_2 gases, an equilibration of pressure takes place and a quantity of gas forms a monolayer over the external surface of the solid. With knowledge of the area covered by each absorbed gas molecule, the surface area of the pores can be determined. The result from the dosage of gas produces the isotherm graphs that help define the type of pores contained in a given sample. In this study, the Green River Formation, Woodford shale and Cameo Coal samples exhibit both monolayer and multi-layer adsorption, which indicates the presence of all three pore sizes; micro-pores, mesopores, and macro-pores. The density functional theory (DFT) model can reduce the isotherm data further to create a continuous distribution of pore volume with respect to pore size (Micrometrics).

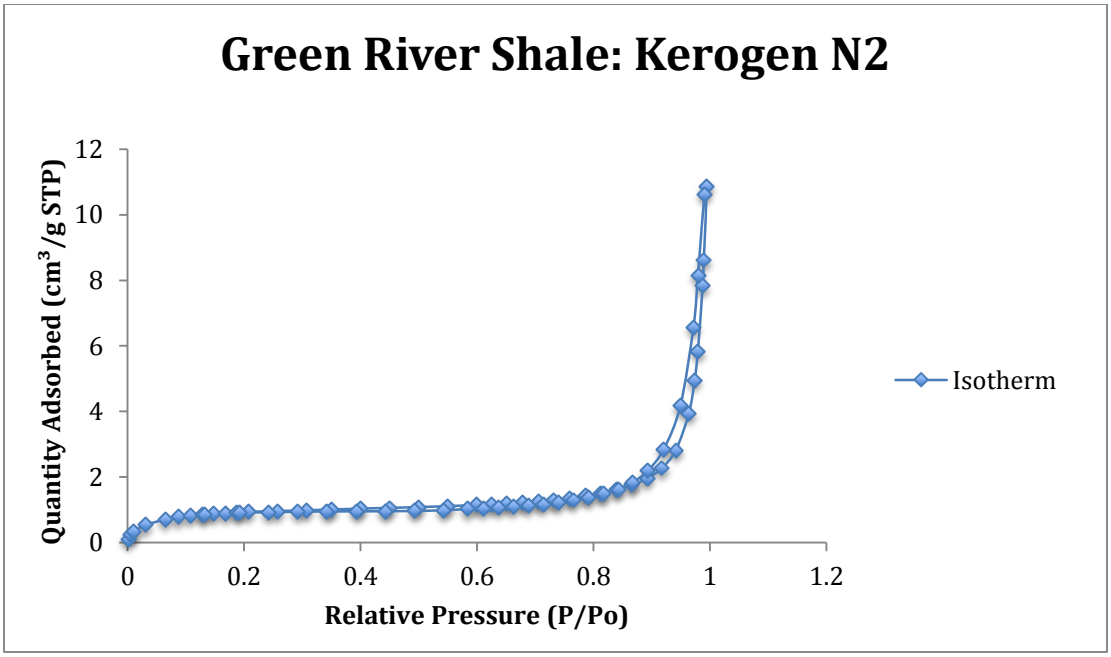

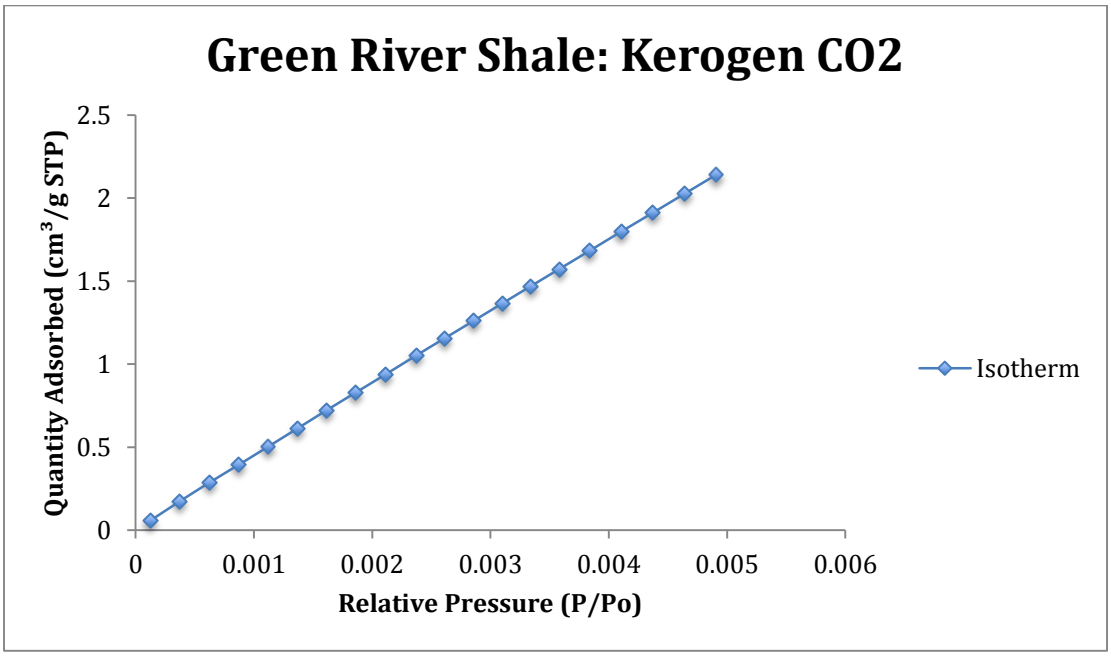

Figure 4.1: Isotherm graphs of N_2 and CO_2 adsorption measurement on Green River shale kerogen.

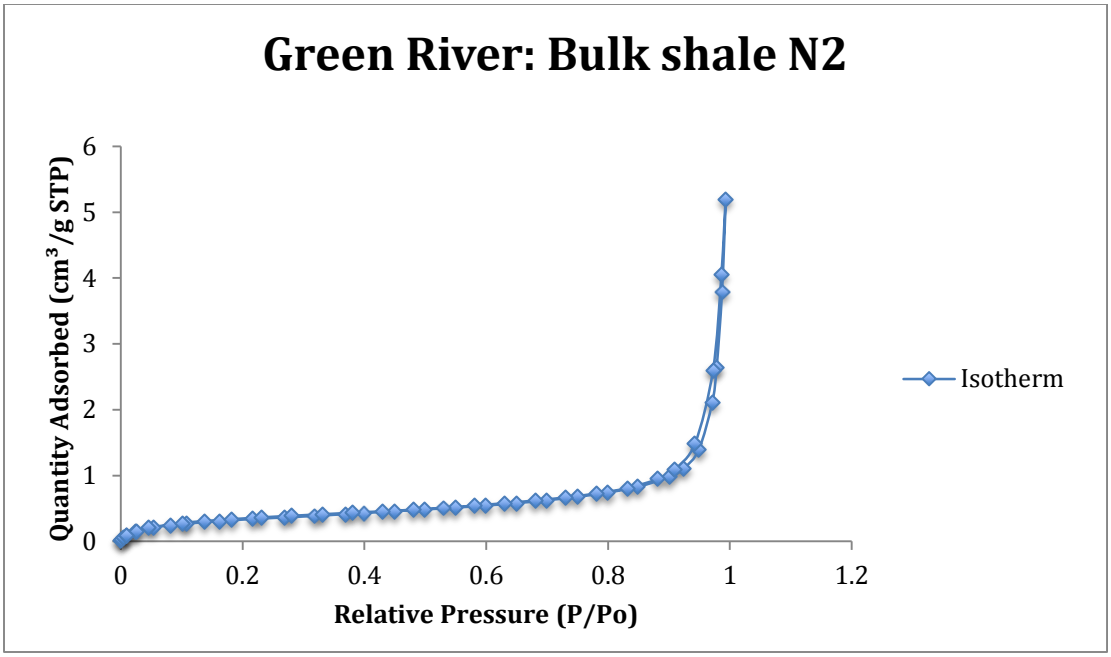

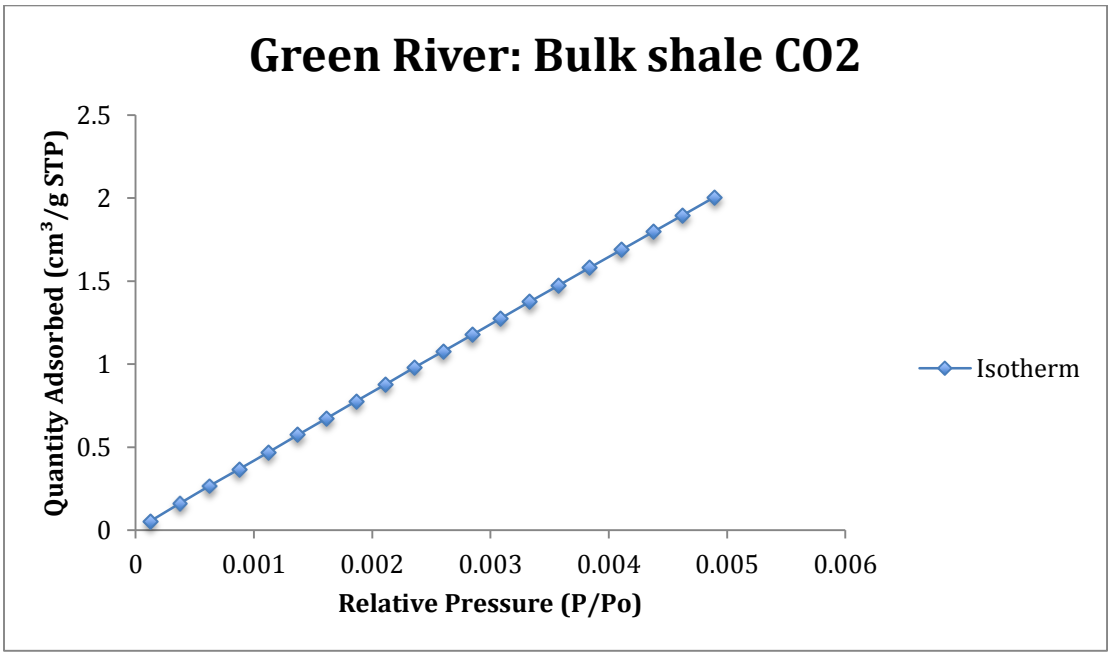

Figure 4.2: Isotherm graphs of N_2 and CO_2 adsorption measurement on Green River bulk shale.

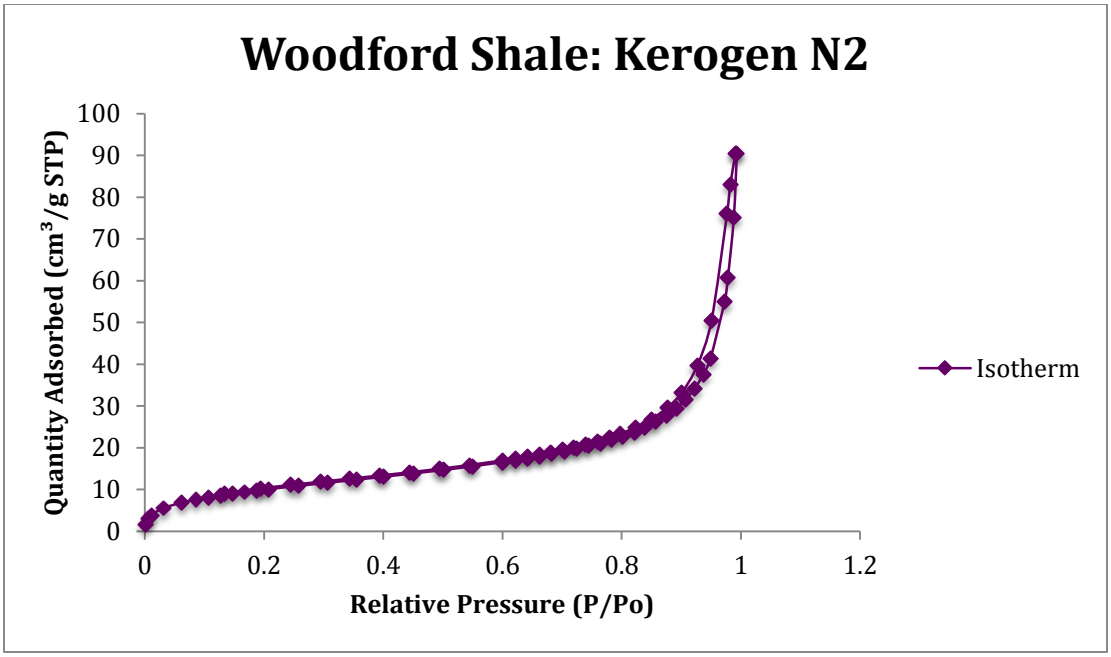

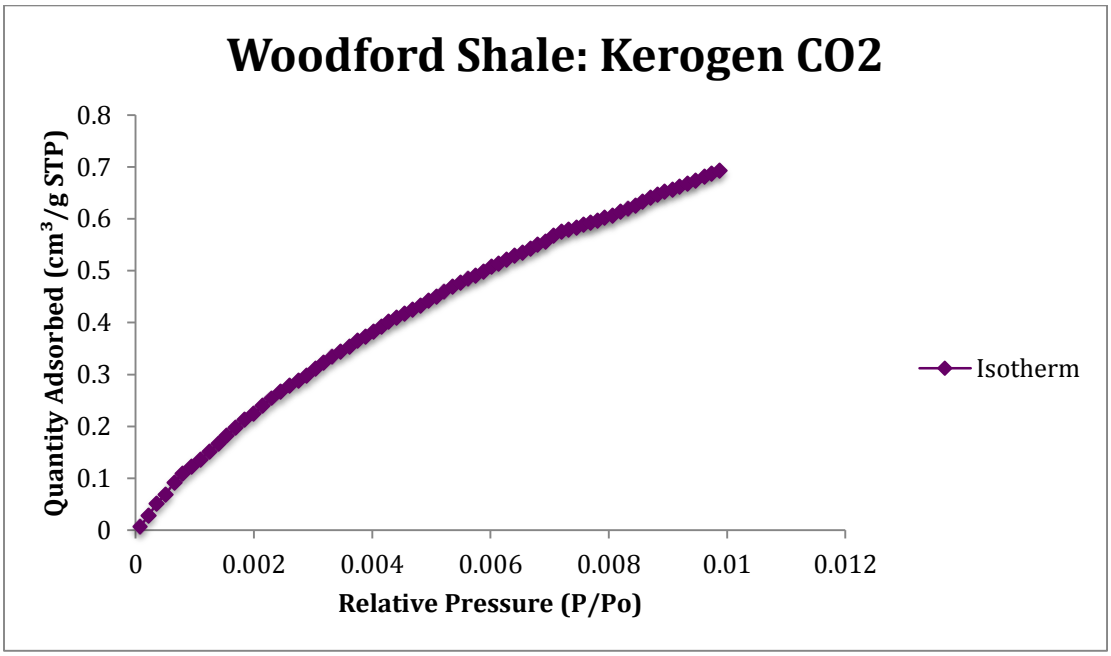

Figure 4.3: Isotherm graphs of N_2 and CO_2 adsorption measurement on Woodford Shale kerogen.

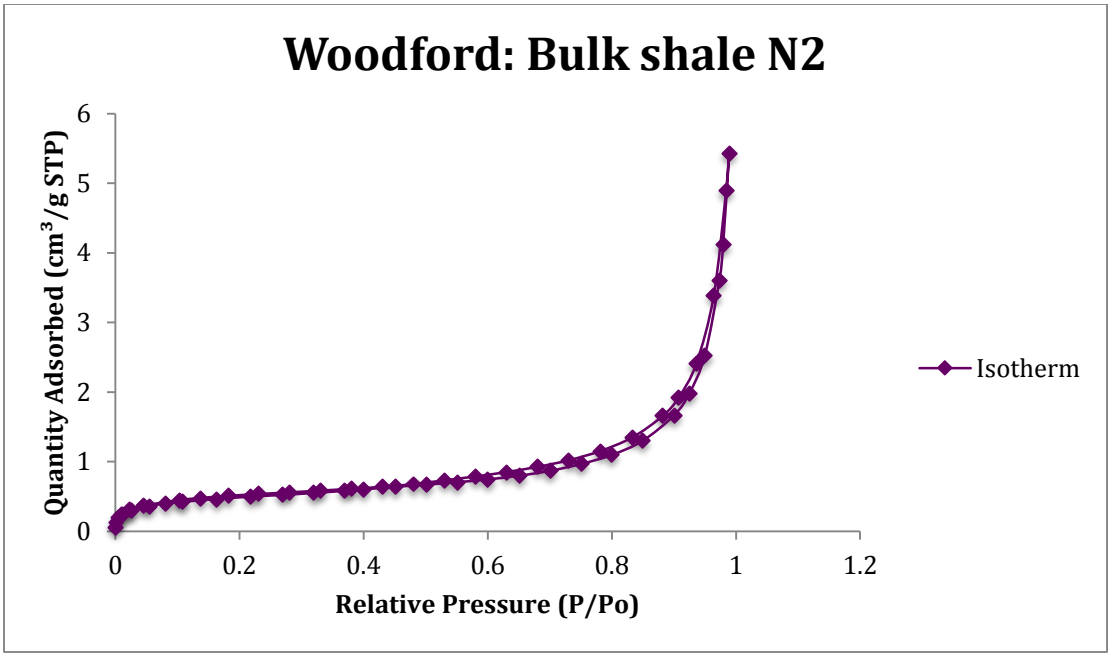

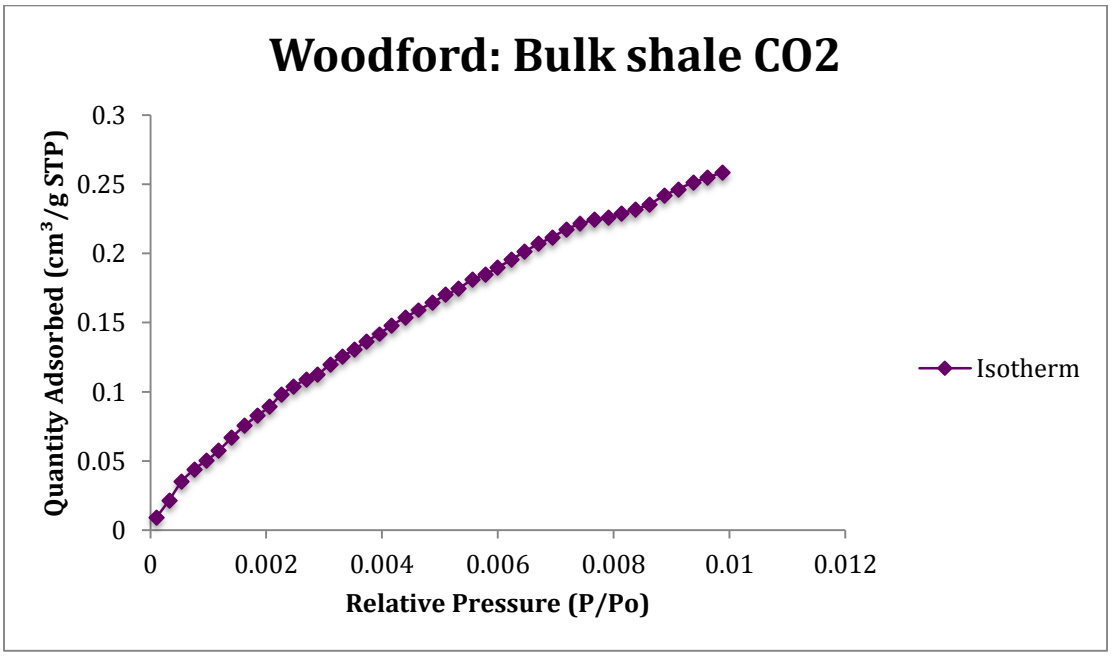

Figure 4.4: Isotherm graphs of N_2 and CO_2 adsorption measurement on Woodford bulk shale.

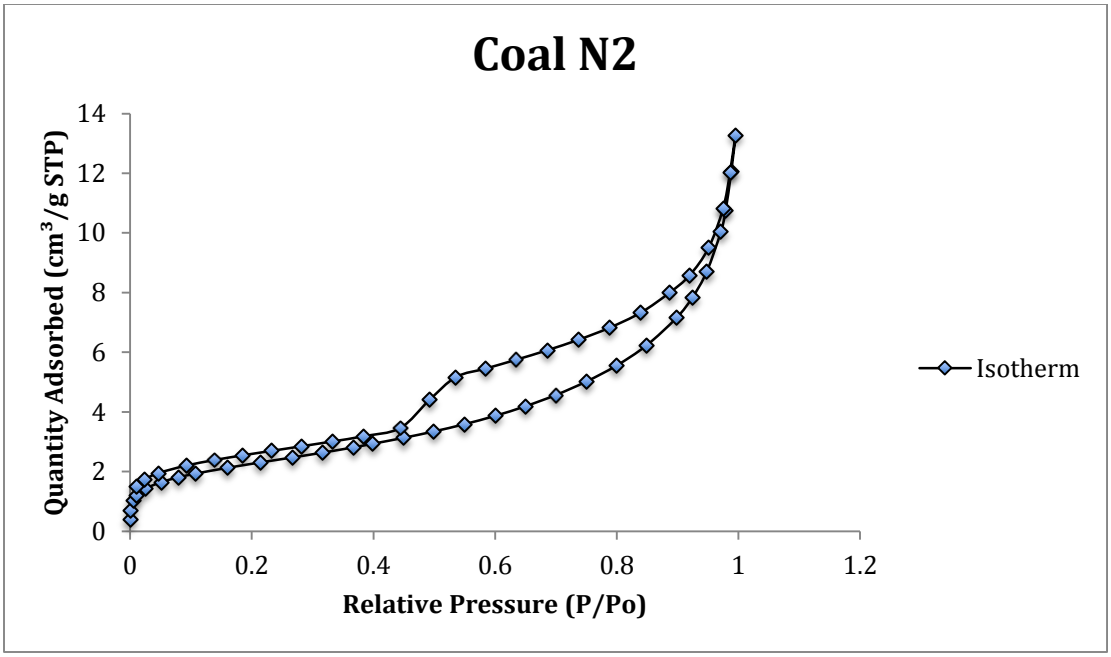

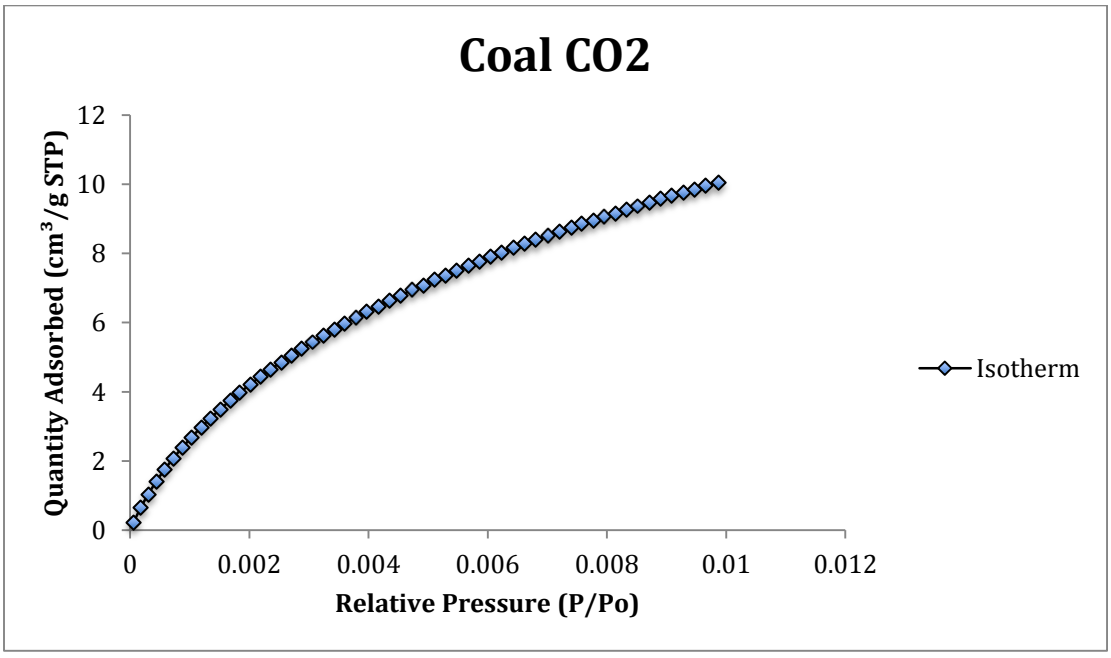

Figure 4.5: Isotherm graphs of N_2 and CO_2 adsorption measurement on Cameo Coal.

The graphs in Figures 4.1 – 4.5 above show the adsorption of N_2 and CO_2 onto the kerogen and bulk shale of Green River and Woodford shales and Cameo coal. The kerogen is known to contain the bulk of the porosity found in these rocks and in these results, the kerogen shows a higher quantity adsorbed compared to the bulk shale. Cameo coal is predominantly made up of organic matter and shows a similar amount of gas adsorbed when compared to the kerogens of the other two shale samples. The isotherm graphs of N_2 adsorption differs from that of CO_2 due to a gap between the equilibrium pressures during adsorption and desorption of the N_2 gas. The N_2 gas adsorption takes place in the mesoporous and macroporous regions of the samples that contain pore sizes above 2 nm. The presence of the hysteresis loop signifies that the mesopore or macro-pore filling varies from the mesopore or macro-pore draining, and indicates that a multilayer adsorption took place. The hysteresis loops displayed in the isotherm graphs above suggest that the pore structure of these samples contain slit-like pores and have a relatively broad range of pore sizes. Since macro-pore filling takes place at relative pressures close to unity, the lack of a hysteresis loop in the CO_2 gas adsorption isotherm graphs is due to the low pressure at which it is run. At such low pressures, the pores that are filled are generally micro-pores that signify a monolayer adsorption.

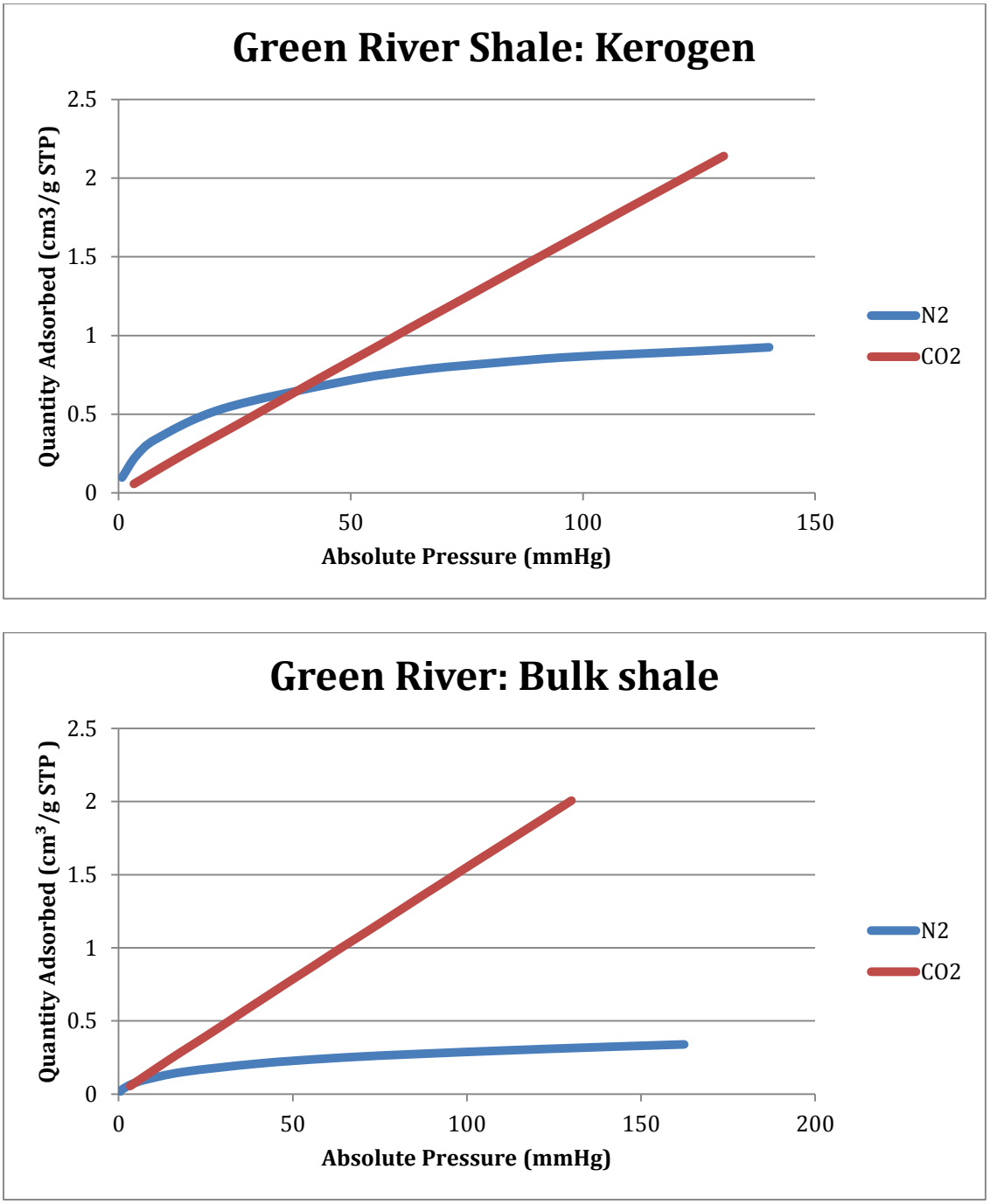

Figure 4.6: Graphs comparing the adsorption capacities obtained from N_2 and CO_2 adsorption measurements on Green River kerogen and bulk shale.

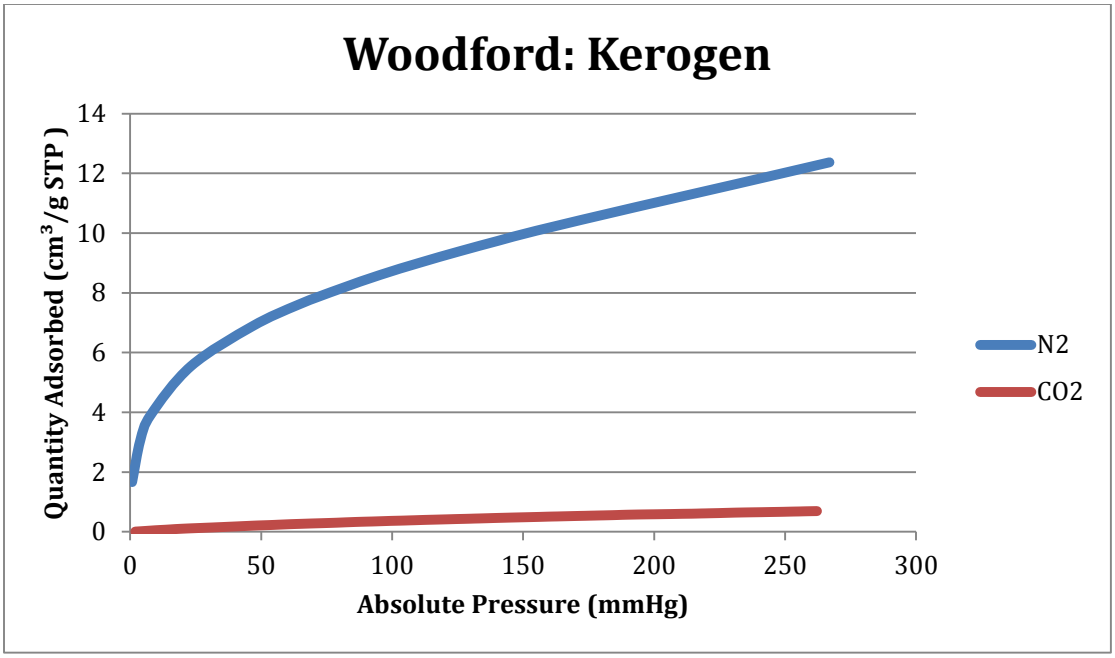

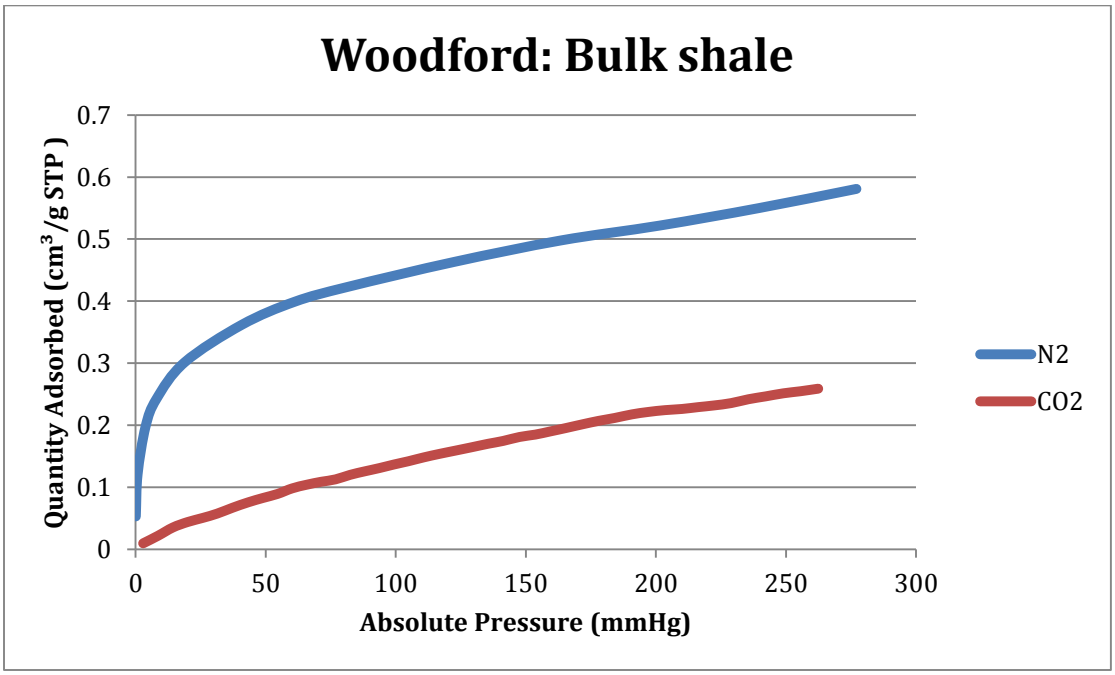

Figure 4.7: Graphs comparing the adsorption capacities obtained from N_2 and CO_2 adsorption measurements on Woodford kerogen and bulk shale.

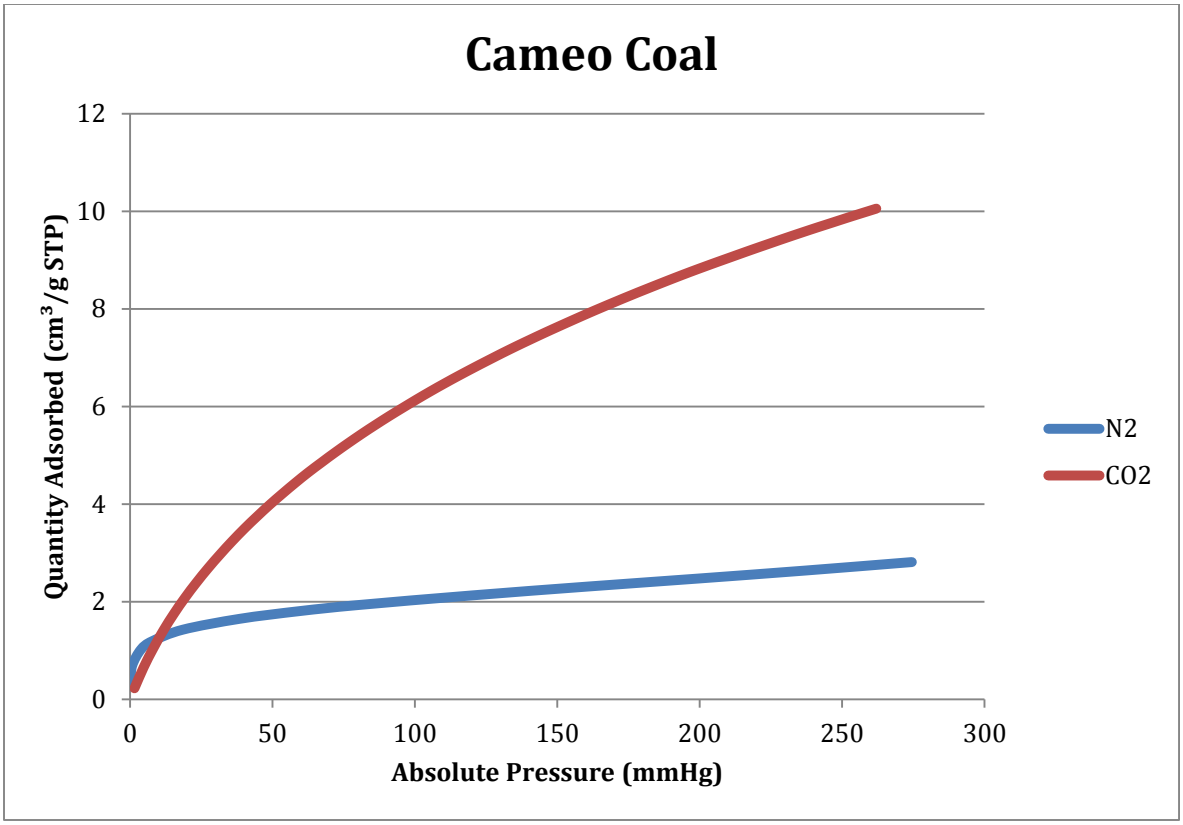

Figure 4.8: Graphs comparing the adsorption capacities obtained from N_2 and CO_2 adsorption measurements on Cameo Coal.

Figures 4.6 – 4.8 show a comparison between the adsorptive capacities of N_2 and CO_2. In Figures 4.6 and 4.8, it can be seen that CO_2 has an adsorptive capacity of about 2 to 3 times that of N_2 in micro-pores at lower pressure. Though Tables A.1 – A.6 show that in larger pore sizes and at higher pressures, the adsorptive capacity of N_2 increases, it can be deduced that N_2 is more efficient at characterizing larger pore sizes. Figure 4.7 draws our attention to a deviation from the norm, with N_2 having a greater adsorptive

capacity than CO_2. This phenomenon may be due to a lack of micro-pores in the Woodford shale as shown in the pore size distribution graph in Figure 4.10.

4.1.1.2. Pore Size Distribution

A low relative pressure is necessary in order to quantify micro-pores in shales. Nitrogen adsorption measurement techniques at 77 K cannot provide this quantification but carbon dioxide at 273 K is an efficient technique for characterizing micro pore sizes. The success of the use of carbon dioxide at 273 K stems from the fact that combination of the high saturation pressure and this temperature allows lower relative pressures. The lower relative pressures enables the carbon dioxide to quantify the micro pores. Adsorption measurements produce isotherm data, shown in Tables A.1 – A.6. We used the density functional theory (DFT) model to manipulate these data to produce the pore size distribution data presented in Tables A.7 – A.8. The pore size distribution graphs below show the results obtained in this study from the low-pressure gas adsorption measurements carried out using N_2 and CO_2 as a ratio of the differential volume to the pore width. These pore size distributions adequately quantify pore sizes that can be used to evaluate the production of hydrocarbons in reservoirs.

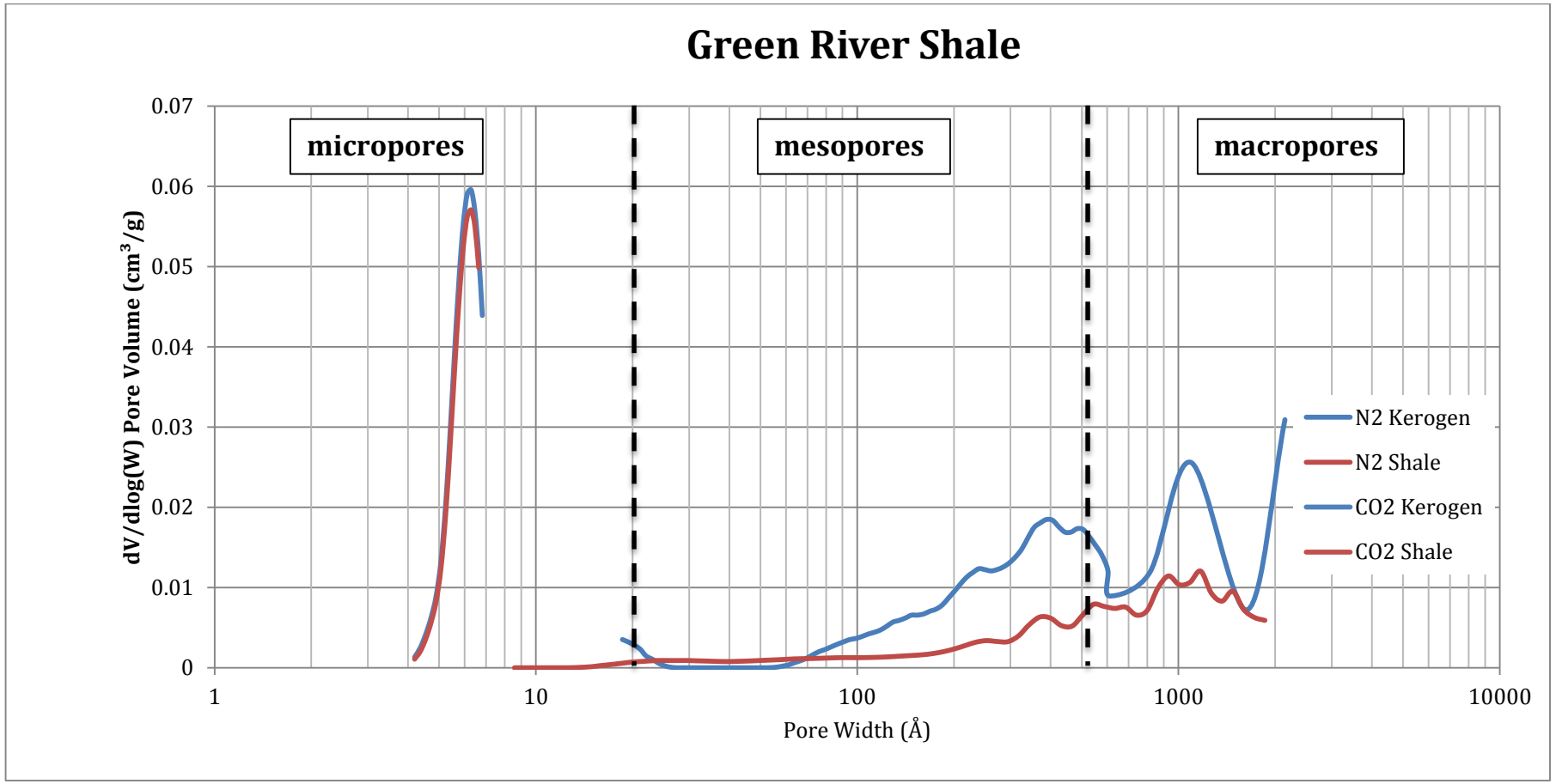

Figure 4.9: Pore size distribution graph of kerogen and bulk shale of Green River Shale.

1 Angstrom (Å) = 10 nm

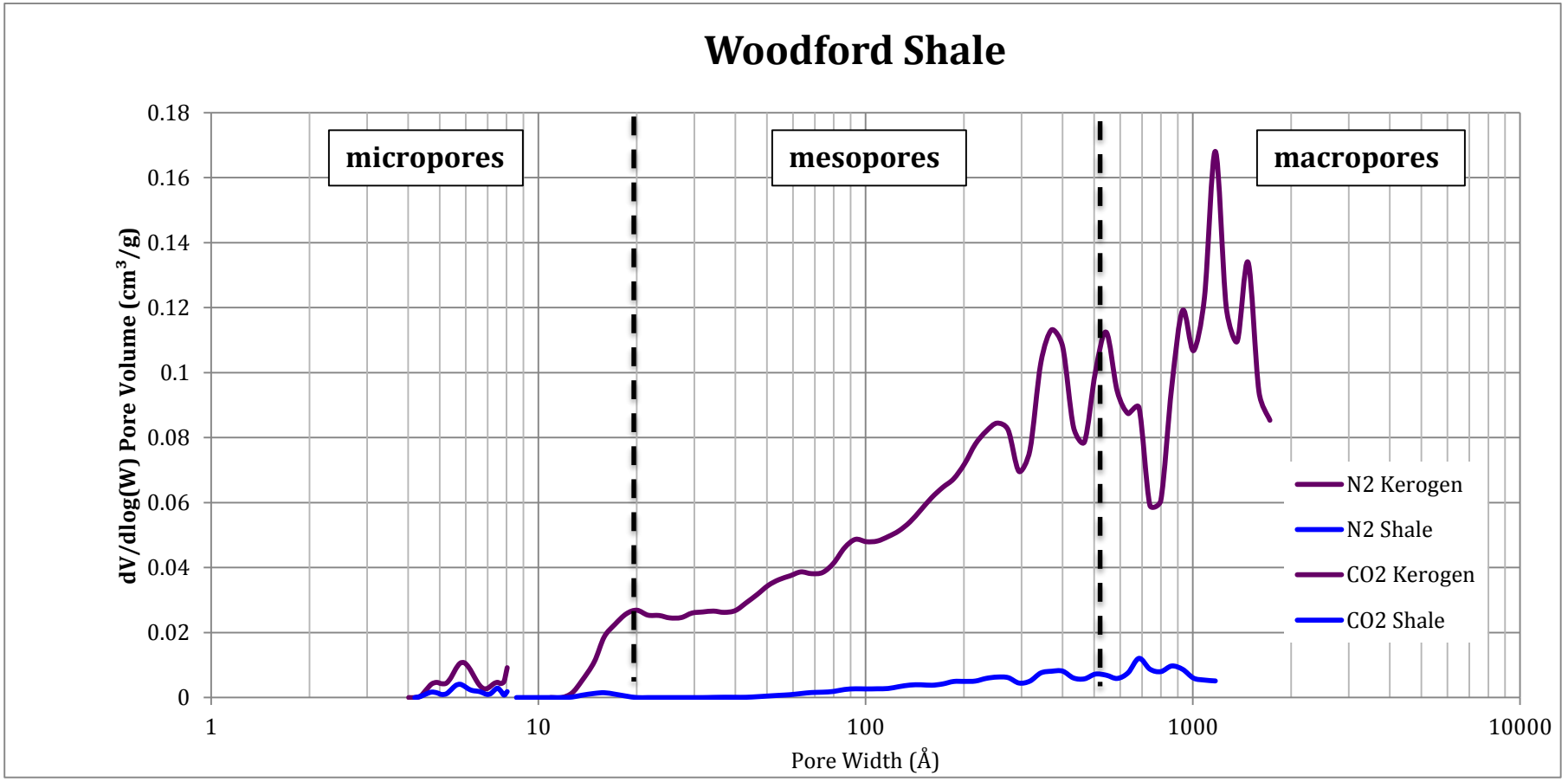

Angstrom (Å) = 10 nm

Figure 4.10: Pore size distribution graph of kerogen and bulk shale of Woodford Shale.

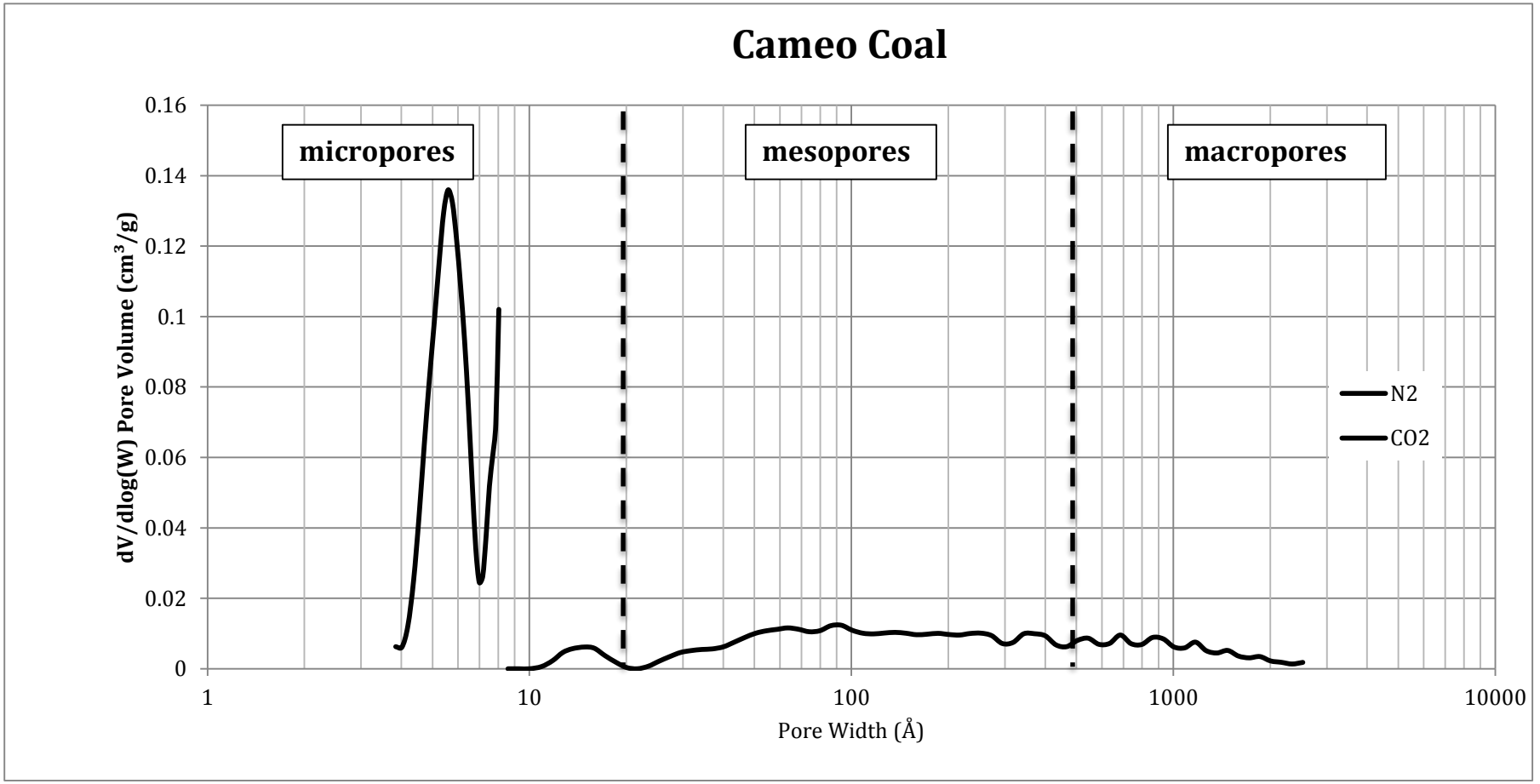

Figure 4.11: Pore size distribution graph of Cameo Coal.

1 Angstrom (Å) = 10 nm

Figures 4.9 – 4.11 above describe the pore size distribution of Green River shale, Woodford shale and Cameo coal. In all three figures, pore sizes range from 0.3 to ~ 300 nm, which aligns with Chalmers et al. investigation of the combined use of CO_2 and N_2 in gas adsorption (Chalmers et al. 2012). The pore sizes are distributed into three categories as follows: (1) Micro-pores which describe pore sizes less than 2 nm, (2) Mesopores which describe pore sizes ranging from 2 nm to 50 nm, and (3) Macro-pores which are associated with pore sizes above 50 nm.

Figures 4.9 and 4.10 contain graphs that indicate variations between the pore sizes found in the kerogen and the bulk shale. It can be seen that the porosity in these samples is found predominantly in the kerogen. Also, the porosity found in kerogens is well distributed across all three pore size categories with the majority of the pores falling below the macro-pore region with the exception of the Woodford shale sample. Figure 4.9 shows that a large percentage of Green River shale's porosity is in the micro porous region, comprising of both kerogen and bulk shale, while the majority of the larger pores is found in the kerogen.

The pore size distribution of Woodford shale is shown in Figure 4.10 and displays an abundance of porosity in the mesopore and macro-pore region of the kerogen. This result can explain the anomaly in the adsorption capacity data of the CO_2 adsorption run, because there is a shortage of micro-pores in this sample. Figure 4.11 describes the pore sizes found in Cameo coal, where the majority of pores found fall in the micro-pore region with additional pore sizes found in the mesoporous and macroporous regions.

CHAPTER 5: CONCLUSION AND RECOMMENDATION

This study was conducted to investigate the pore size and structure of organic matter (OM) hosted rocks. The samples used included (1) The kerogen and bulk shale of Green River shale, (2) The kerogen and bulk shale of Woodford shale, and (3) Cameo Coal. Using a 3Flex Porosimeter, we carried out adsorption measurements on each sample. The isotherm data gotten from the adsorption measurements were manipulated using the density functional theory (DFT) model to construct pore size distributions. The results confirm that over 50% of the porosity in the OM-hosted samples above are contained in pores smaller than the seismic electron microscope (SEM) limit of ~ 5 nm with the exception of Woodford shale, where the predominant of porosity is contained in pore sizes above this limit.

From the results, CO_2 proved to be efficient in capturing pore sizes as small as 0.3 nm, while N_2 was efficient in quantifying pores that fell into the mesopore and macro-pore size regions. The combined use of CO_2 and N_2 in low-pressure gas adsorption to investigate the pore sizes of the OM-hosted samples enabled us to expand the range of pore sizes.

It was necessary to identify the pore size distribution of these samples to observe the type of material in the rock that makes up the bulk of the porosity, which we found to be the kerogen, which is also a host to much of the producible hydrocarbon. Having the majority of pores in the kerogen tells us that permeability will be highly dependent on the pore sizes of the kerogen. To evaluate the relationship between permeability and the pore

size distribution of the samples used, we calculated the approximate maximum permeability existing in these samples using a manipulation of the diffusive mass transfer equation from (Singh et al. 2014). For an average pore diameter of 100 nm, we used their Eq. 17 assuming the flow of methane, at an average pressure of 20 MPa, a temperature of 400 K and a porosity of ~ 5 %, a value derived from the results of the adsorption measurement, and found the approximate maximum permeability in these samples to be ~ 2 μD (Singh et al. 2014). The absolute permeability of the shale will depend on the connectivity of the kerogen pores to the inorganic matrix as well as their size distribution but this value represents a theoretical maximum. The knowledge of the quantity of porosity, pore sizes, and the distribution of these pore sizes will aid in predicting the oil-in-place and controlling the flow of hydrocarbon from such shale reservoirs.

Based on this understanding, we recommend that rocks be allowed to reach an optimal thermal maturity in order to harness as much organic matter as possible to allow maximum rock porosity and hence, hydrocarbon production.

In support to the work of (Liu & Seaton 1994), we recommend that an investigation into the connectivity between the pores in the kerogen and the pores in the bulk shales/rocks will be essential in determining the transport of matter and reaction between these pores. Ultimately, an investigation into the pore connectivity will generate a more efficient process in hydrocarbon production and recovery from OM-hosted rocks.

APPENDIX

The data collected from the adsorption measurements in this study are presented in this chapter. These measurements include the carbon dioxide and nitrogen adsorption data, which after manipulation constitute the pore size distribution. The data collected from the adsorption measurements in this study are presented in this chapter. These measurements include the carbon dioxide and nitrogen adsorption data, which after manipulation constitute the pore size distribution.

Green River Shale					
Kerogen			Bulk Shale		
Relative Pressure (P/Po)	Absolute Pressure (mmHg)	Quantity Adsorbed (cm^3/g STP)	Relative Pressure (P/Po)	Absolute Pressure (mmHg)	Quantity Adsorbed (cm^3/g STP)
0.0001	3.2960	0.0576	0.0001	3.3248	0.0549
0.0004	9.9137	0.1738	0.0004	9.9536	0.1616
0.0006	16.5662	0.2868	0.0006	16.5905	0.2668
0.0009	23.1116	0.3934	0.0009	23.2276	0.3673
0.0011	29.7143	0.5023	0.0011	29.8354	0.4694
0.0014	36.3036	0.6121	0.0014	36.4256	0.5734
0.0016	42.8378	0.7214	0.0016	42.9671	0.6750
0.0019	49.4037	0.8287	0.0019	49.5472	0.7776
0.0021	56.0808	0.9376	0.0021	56.1148	0.8779
0.0024	62.9565	1.0515	0.0024	62.5406	0.9787
0.0026	69.4026	1.1559	0.0026	69.0476	1.0769
0.0029	75.8552	1.2602	0.0028	75.5482	1.1758
0.0031	82.3026	1.3654	0.0031	82.0105	1.2760
0.0033	88.7171	1.4692	0.0033	88.4553	1.3753
0.0036	95.1387	1.5729	0.0036	94.8542	1.4721
0.0038	101.8590	1.6815	0.0038	101.8677	1.5797
0.0041	109.0132	1.7979	0.0041	109.0240	1.6876
0.0044	116.1408	1.9118	0.0044	116.2465	1.7969
0.0046	123.3405	2.0277	0.0046	122.8245	1.8966
0.0049	130.3058	2.1398	0.0049	130.0152	2.0062

Table A.1: Isotherm Data for Green River kerogen and bulk shale CO_2 gas adsorption.

Woodford Shale					
Kerogen			Bulk Shale		
Relative Pressure (P/Po)	Absolute Pressure (mmHg)	Quantity Adsorbed (cm^3/g STP)	Relative Pressure (P/Po)	Absolute Pressure (mmHg)	Quantity Adsorbed (cm^3/g STP)
0.0001	1.9493	0.0067	0.0001	2.8880	0.0095
0.0002	5.7792	0.0281	0.0003	8.5916	0.0217
0.0004	9.6017	0.0516	0.0005	14.3022	0.0351
0.0005	13.4456	0.0694	0.0008	19.9913	0.0439
0.0007	17.3116	0.0913	0.0010	25.7242	0.0504
0.0008	21.2042	0.1088	0.0012	31.3525	0.0575
0.0009	25.1144	0.1229	0.0014	37.2932	0.0670
0.0011	29.0375	0.1368	0.0016	43.2385	0.0756
0.0012	33.0012	0.1513	0.0018	48.9424	0.0827
0.0014	36.9630	0.1665	0.0021	54.5521	0.0892
0.0015	40.9469	0.1820	0.0023	60.1516	0.0981
0.0017	44.9475	0.1982	0.0025	65.7542	0.1040
0.0018	48.9451	0.2129	0.0027	71.3340	0.1088
0.0020	52.9909	0.2249	0.0029	76.8401	0.1127
0.0021	57.0351	0.2397	0.0031	82.4481	0.1199
0.0023	61.0587	0.2547	0.0033	87.9755	0.1255
0.0025	65.1240	0.2667	0.0035	93.7413	0.1309
0.0026	69.0407	0.2779	0.0037	99.3246	0.1367
0.0027	72.9583	0.2878	0.0039	104.8341	0.1419
0.0029	76.8708	0.2988	0.0042	110.7828	0.1481
0.0030	80.6528	0.3113	0.0044	116.9695	0.1539
0.0032	84.2303	0.3241	0.0046	122.9287	0.1590

Woodford Shale					
Kerogen			Bulk Shale		
Relative Pressure (P/Po)	Absolute Pressure (mmHg)	Quantity Adsorbed (cm^3/g STP)	Relative Pressure (P/Po)	Absolute Pressure (mmHg)	Quantity Adsorbed (cm^3/g STP)
0.0035	92.1447	0.3447	0.0051	135.5103	0.1700
0.0036	95.9199	0.3547	0.0053	141.2654	0.1746
0.0037	99.5350	0.3653	0.0056	147.6002	0.1810
0.0039	103.1065	0.3731	0.0058	153.6395	0.1849
0.0040	106.7130	0.3823	0.0060	159.3588	0.1899
0.0042	110.3362	0.3925	0.0062	165.5131	0.1955
0.0043	113.8106	0.4017	0.0065	171.5453	0.2012
0.0044	117.3511	0.4096	0.0067	177.9646	0.2070
0.0045	120.8239	0.4176	0.0069	184.1871	0.2117
0.0047	124.3196	0.4263	0.0072	190.6879	0.2174
0.0048	127.7623	0.4337	0.0074	196.9884	0.2213
0.0050	131.6013	0.4431	0.0077	203.5130	0.2243
0.0051	135.0285	0.4511	0.0079	210.0570	0.2262
0.0052	138.4114	0.4600	0.0081	216.2624	0.2291
0.0054	142.2619	0.4695	0.0084	222.2386	0.2318
0.0055	145.8041	0.4771	0.0086	228.9097	0.2356
0.0056	149.2715	0.4846	0.0089	235.5669	0.2418
0.0058	152.7221	0.4917	0.0091	242.2330	0.2465
0.0059	156.1035	0.4986	0.0094	248.9908	0.2514
0.0060	159.5542	0.5076	0.0096	255.6046	0.2548
0.0061	162.9740	0.5140	0.0099	262.3591	0.2588
0.0063	166.2851	0.5209			
0.0064	170.1821	0.5291			

Woodford Shale		
Kerogen		
Relative Pressure (P/Po)	Absolute Pressure (mmHg)	Quantity Adsorbed (cm^3/g STP)
0.0065	173.6386	0.5356
0.0067	177.3677	0.5436
0.0068	180.5968	0.5499
0.0071	187.7310	0.5671
0.0072	191.1622	0.5746
0.0073	194.3641	0.5800
0.0075	198.0210	0.5842
0.0076	201.2881	0.5882
0.0077	204.4381	0.5923
0.0078	207.6330	0.5968
0.0079	210.7856	0.6024
0.0081	214.2580	0.6055
0.0082	217.8804	0.6135
0.0083	221.1107	0.6200
0.0085	224.5300	0.6268
0.0086	227.6685	0.6341
0.0087	231.0869	0.6422
0.0088	234.3226	0.6476
0.0089	237.4573	0.6521
0.0091	240.9973	0.6570
0.0092	244.2329	0.6618
0.0093	247.9782	0.6676
0.0095	251.1992	0.6737
0.0096	255.3492	0.6812
0.0097	258.5047	0.6879
0.0099	262.1459	0.6935

Table A.2: Isotherm Data for Woodford kerogen and bulk shale CO_2 gas adsorption.

Cameo Coal		
Relative Pressure (P/Po)	Absolute Pressure (mmHg)	Quantity Adsorbed (cm^3/g STP)
0.0001	1.5034	0.2248
0.0002	4.6959	0.6499
0.0003	8.0931	1.0409
0.0004	11.6685	1.4109
0.0006	15.4082	1.7567
0.0007	19.2614	2.0814
0.0009	23.2540	2.3900
0.0010	27.3332	2.6836
0.0012	31.5555	2.9672
0.0013	35.7817	3.2369
0.0015	40.1383	3.4980
0.0017	44.5269	3.7444
0.0018	48.9296	3.9818
0.0020	53.4238	4.2102
0.0022	57.9652	4.4332
0.0024	62.5621	4.6490
0.0025	67.2687	4.8558
0.0027	71.9281	5.0564
0.0029	76.5872	5.2484
0.0031	81.3295	5.4382
0.0032	86.1235	5.6218
0.0034	90.9335	5.8006
0.0036	95.7021	5.9716
0.0038	100.5914	6.1433
0.0040	105.4673	6.3097
0.0042	110.5560	6.4769
0.0043	115.4847	6.6335
0.0045	120.3562	6.7840
0.0047	125.6293	6.9428
0.0049	130.5747	7.0898
0.0051	135.4424	7.2297
0.0053	140.3707	7.3670
0.0055	145.2766	7.5011
0.0057	150.6497	7.6438
0.0059	155.5691	7.7730
0.0060	160.4761	7.8994

Cameo Coal		
Relative Pressure (P/Po)	Absolute Pressure (mmHg)	Quantity Adsorbed (cm^3/g STP)
0.0064	170.8519	8.1568
0.0066	175.7872	8.2763
0.0068	180.7633	8.3937
0.0070	186.2483	8.5210
0.0072	191.1669	8.6335
0.0074	196.4009	8.7503
0.0076	201.3134	8.8566
0.0078	206.2308	8.9605
0.0080	211.1882	9.0637
0.0081	216.2522	9.1695
0.0083	221.1118	9.2686
0.0085	226.0641	9.3691
0.0087	231.3553	9.4751
0.0089	236.4512	9.5748
0.0091	241.2822	9.6676
0.0093	246.5221	9.7661
0.0095	251.4176	9.8591
0.0097	256.4861	9.9522
0.0099	261.9912	10.0527

Table A.3: Isotherm Data for Cameo Coal CO_2 gas adsorption.

Green River Shale							
Kerogen				Bulk Shale			
Adsorption		Desorption		Adsorption		Desorption	
Relative Pressure (P/Po)	Quantity Adsorbed (cm^3/g STP)	Relative Pressure (P/Po)	Quantity Adsorbed (cm^3/g STP)	Relative Pressure (P/Po)	Quantity Adsorbed (cm^3/g STP)	Relative Pressure (P/Po)	Quantity Adsorbed (cm^3/g STP)
0.0010	0.0983	0.9944	10.8789	0.0002	0.0095	0.9931	5.1925
0.0051	0.2357	0.9903	10.6206	0.0011	0.0279	0.9861	4.0502
0.0106	0.3398	0.9793	8.1539	0.0049	0.0663	0.9724	2.6024
0.0299	0.5346	0.9715	6.5706	0.0098	0.0953	0.9428	1.4860
0.0647	0.7072	0.9490	4.1730	0.0249	0.1515	0.9093	1.0923
0.0867	0.7812	0.9206	2.8543	0.0537	0.2085	0.8817	0.9469
0.1076	0.8246	0.8933	2.1978	0.0810	0.2438	0.8312	0.8082
0.1277	0.8601	0.8675	1.8437	0.1084	0.2692	0.7811	0.7280
0.1475	0.8818	0.8423	1.6328	0.1624	0.3072	0.7305	0.6677
0.1676	0.9017	0.8170	1.4887	0.2168	0.3393	0.6803	0.6208
0.1876	0.9252	0.7918	1.3856	0.2689	0.3627	0.6302	0.5800
0.2074	0.9414	0.7654	1.2989	0.3186	0.3864	0.5801	0.5426
0.2573	0.9626	0.7393	1.2268	0.3684	0.4125	0.5302	0.5085
0.3071	0.9868	0.7136	1.1754	0.3994	0.4299	0.4801	0.4809
0.3494	1.0087	0.6877	1.1300	0.4491	0.4569	0.4301	0.4567
0.3994	1.0381	0.6620	1.1000	0.4992	0.4841	0.3804	0.4349
0.4494	1.0593	0.6363	1.0733	0.5491	0.5120	0.3302	0.4115
0.4994	1.0845	0.6100	1.0490	0.5993	0.5433	0.2803	0.3885
0.5495	1.1120	0.5836	1.0255	0.6492	0.5797	0.2304	0.3636
0.5992	1.1506	0.5424	0.9872	0.6991	0.6232	0.1825	0.3368
0.6253	1.1660	0.4923	0.9653	0.7492	0.6760	0.1370	0.3076
0.6511	1.1948	0.4423	0.9588	0.7994	0.7414	0.1021	0.2780

Green River Shale							
Kerogen				Bulk Shale			
Adsorption		Desorption		Adsorption		Desorption	
Relative Pressure (P/Po)	Quantity Adsorbed (cm^3/g STP)	Relative Pressure (P/Po)	Quantity Adsorbed (cm^3/g STP)	Relative Pressure (P/Po)	Quantity Adsorbed (cm^3/g STP)	Relative Pressure (P/Po)	Quantity Adsorbed (cm^3/g STP)
0.6781	1.2204	0.3924	0.9523	0.8492	0.8290	0.0458	0.2077
0.7053	1.2598	0.3422	0.9517	0.9007	0.9789	0.0257	0.1587
0.7317	1.3003	0.2922	0.9406	0.9243	1.1089	0.0093	0.0923
0.7589	1.3575	0.2422	0.9271	0.9490	1.3930		
0.7858	1.4241	0.1922	0.9102	0.9710	2.1076		
0.8124	1.5088	0.1322	0.8627	0.9782	2.6356		
0.8392	1.6196			0.9871	3.7857		
0.8658	1.7583			0.9931	5.1925		
0.8923	1.9586						
0.9171	2.2718						
0.9412	2.8225						
0.9636	3.9447						
0.9735	4.9462						
0.9791	5.8411						
0.9873	7.8339						
0.9893	8.6254						
0.9944	10.8789						

Table A.4: Isotherm Data for Green River kerogen and bulk shale N_2 gas adsorption.

Woodford Kerogen Adsorption		Woodford Kerogen Desorption		Woodford Bulk Shale Adsorption		Woodford Bulk Shale Desorption	
Relative Pressure (P/Po)	Quantity Adsorbed (cm^3/g STP)	Relative Pressure (P/Po)	Quantity Adsorbed (cm^3/g STP)	Relative Pressure (P/Po)	Quantity Adsorbed (cm^3/g STP)	Relative Pressure (P/Po)	Quantity Adsorbed (cm^3/g STP)
0.0010	1.6647	0.9929	90.5646	0.0001	0.0530	0.9889	5.4311
0.0051	3.0508	0.9911	90.4400	0.0010	0.1210	0.9840	4.8894
0.0104	3.9125	0.9821	82.9594	0.0051	0.1975	0.9640	3.3811
0.0310	5.5450	0.9766	76.0110	0.0107	0.2422	0.9360	2.4078
0.0622	6.8790	0.9506	50.5031	0.0251	0.3013	0.9079	1.9256
0.0859	7.6089	0.9264	39.5778	0.0545	0.3619	0.8820	1.6588
0.1072	8.1400	0.9003	33.1197	0.0816	0.3990	0.8334	1.3509
0.1272	8.5975	0.8760	29.5476	0.1088	0.4229	0.7817	1.1542
0.1474	9.0069	0.8501	26.8761	0.1634	0.4632	0.7308	1.0207
0.1675	9.3878	0.8228	24.8327	0.2183	0.4979	0.6804	0.9258
0.1876	9.7461	0.7972	23.3383	0.2689	0.5218	0.6305	0.8511
0.2068	10.0802	0.7789	22.4126	0.3198	0.5500	0.5800	0.7868
0.2571	10.8650	0.7597	21.5831	0.3698	0.5809	0.5303	0.7325
0.3069	11.6177	0.7396	20.7910	0.4000	0.6014	0.4802	0.6772
0.3560	12.3687	0.7198	20.0983	0.4511	0.6388	0.4302	0.6386
0.4004	13.0589	0.7007	19.4882	0.5010	0.6698	0.3800	0.6100
0.4508	13.8591	0.6812	18.9285	0.5504	0.7046	0.3302	0.5842
0.5005	14.6798	0.6614	18.4054	0.6002	0.7453	0.2801	0.5588
0.5494	15.5545	0.6416	17.9044	0.6509	0.7984	0.2303	0.5344
0.6000	16.5473	0.6215	17.4414	0.7006	0.8683	0.1824	0.5090
0.6213	17.0144	0.6000	16.9681	0.7509	0.9680	0.1369	0.4778
0.6423	17.4901	0.5443	15.8611	0.7993	1.0956	0.1025	0.4461

Table A.5: Isotherm Data for Woodford kerogen and bulk shale N_2 gas adsorption.

Cameo Coal			
Adsorption		Desorption	
Relative Pressure (P/Po)	Quantity Adsorbed (cm^3/g STP)	Relative Pressure (P/Po)	Quantity Adsorbed (cm^3/g STP)
0.0010	0.7058	0.9939	12.1960
0.0050	1.0307	0.9909	12.1123
0.0107	1.2044	0.9815	11.2278
0.0303	1.4792	0.9746	10.5889
0.0638	1.7014	0.9470	9.0926
0.0864	1.8126	0.9243	8.4400
0.1075	1.9005	0.8977	7.8935
0.1277	1.9775	0.8718	7.4908
0.1476	2.0475	0.8461	7.1621
0.1677	2.1165	0.8206	6.8850
0.1878	2.1822	0.7951	6.6447
0.2074	2.2457	0.7181	6.0702
0.2559	2.3857	0.6401	5.5904
0.3061	2.5338	0.5611	5.1452
0.3558	2.6968	0.5438	5.0414
0.3992	2.8462	0.4971	4.6200
0.4495	3.0303	0.4448	3.3228
0.4994	3.2317	0.3949	3.0505
0.5494	3.4617	0.3438	2.8771
0.5993	3.7257	0.2937	2.7243
0.6773	4.2245	0.2434	2.5781
0.7537	4.8713	0.1934	2.4333
0.8280	5.7085	0.1327	2.2401
0.8986	6.8921		
0.9609	8.8952		
0.9727	9.6440		
0.9797	10.2036		
0.9880	11.1836		
0.9939	12.1960		

Table A.6: Isotherm Data for Cameo Coal N_2 gas adsorption.

Green River Shale			
Kerogen		Bulk Shale	
Pore Width (Å)	dV/dlog(W) Pore Volume (cm³/g)	Pore Width (Å)	dV/dlog(W) Pore Volume (cm³/g)
4.1928	0.0013	4.1928	0.0011
4.3675	0.0025	4.3675	0.0020
4.5422	0.0042	4.5422	0.0036
4.7169	0.0062	4.7169	0.0056
4.8916	0.0089	4.8916	0.0082
5.0663	0.0133	5.0663	0.0124
5.2410	0.0204	5.2410	0.0192
5.4157	0.0297	5.4157	0.0280
5.5904	0.0396	5.5904	0.0374
5.7651	0.0485	5.7651	0.0458
5.9398	0.0552	5.9398	0.0523
6.1145	0.0590	6.1145	0.0562
6.2892	0.0595	6.2892	0.0571
6.4639	0.0568	6.4639	0.0550
6.6386	0.0515	6.6386	0.0499
6.8133	0.0439	8.5781	0.0000
18.5940	0.0035	9.2929	0.0000
19.4509	0.0032	10.0077	0.0000
20.3078	0.0028	10.9013	0.0000
21.1647	0.0023	11.7948	0.0000
22.0216	0.0015	12.6884	0.0000
23.1641	0.0010	13.5819	0.0000
24.0211	0.0006	14.8329	0.0001
25.1636	0.0002	15.9052	0.0003
26.3061	0.0001	17.1561	0.0004
27.4487	0.0000	18.5858	0.0006
28.8769	0.0000	20.0155	0.0007
30.0194	0.0000	21.6239	0.0008
31.4476	0.0000	23.4110	0.0009
32.8758	0.0000	25.1980	0.0009
34.3040	0.0000	27.3426	0.0009
36.0178	0.0000	29.4871	0.0009
37.4459	0.0000	31.8103	0.0009
39.1598	0.0000	34.3122	0.0008

Green River Shale			
Kerogen		Bulk Shale	
Pore Width (Å)	dV/dlog(W) Pore Volume (cm^3/g)	Pore Width (Å)	dV/dlog(W) Pore Volume (cm^3/g)
41.1592	0.0000	36.9929	0.0008
42.8730	0.0000	40.0309	0.0008
44.8725	0.0000	43.2477	0.0008
46.8719	0.0000	46.6432	0.0009
48.8714	0.0000	50.3961	0.0009
51.1565	0.0000	54.3277	0.0010
53.4416	0.0000	58.7954	0.0010
56.0123	0.0001	63.4419	0.0011
58.2974	0.0002	68.4458	0.0011
61.1537	0.0004	73.9858	0.0012
63.7245	0.0006	79.8832	0.0012
66.5808	0.0009	86.3167	0.0012
69.7228	0.0012	93.1077	0.0013
72.8648	0.0016	100.6135	0.0013
76.0068	0.0020	108.6554	0.0013
79.4344	0.0023	117.2335	0.0013
83.1477	0.0026	126.5264	0.0014
86.8610	0.0029	136.7128	0.0015
90.8599	0.0032	147.6141	0.0015
94.8588	0.0035	159.4089	0.0016
99.1433	0.0037	172.0973	0.0018
103.7135	0.0039	185.8579	0.0020
108.2837	0.0042	200.6908	0.0023
113.1395	0.0044	216.5960	0.0028
118.2809	0.0047	233.9308	0.0032
123.7080	0.0052	252.5166	0.0034
129.1351	0.0057	272.7108	0.0033
134.8478	0.0059	294.5134	0.0033
141.1318	0.0062	317.9243	0.0040
147.4158	0.0066	343.3011	0.0054
153.9854	0.0066	370.6436	0.0063
161.1263	0.0067	400.3094	0.0062
168.2672	0.0070	432.2984	0.0053

Green River Shale			
Kerogen		Bulk Shale	
Pore Width (Å)	dV/dlog(W) Pore Volume (cm^3/g)	Pore Width (Å)	dV/dlog(W) Pore Volume (cm^3/g)
175.6938	0.0073	466.7894	0.0052
183.6916	0.0078	503.9609	0.0066
191.9750	0.0086	544.1706	0.0079
200.5441	0.0095	587.5970	0.0076
209.6845	0.0104	634.4189	0.0074
219.1104	0.0113	684.9937	0.0076
229.1077	0.0119	739.6788	0.0066
239.3906	0.0123	798.6530	0.0071
249.9591	0.0122	862.4523	0.0099
261.3846	0.0121	931.2554	0.0114
273.0956	0.0122	1005.5987	0.0104
285.3780	0.0126	1085.6605	0.0106
298.2316	0.0131	1172.3347	0.0120
311.6565	0.0139	1265.7998	0.0093
325.6527	0.0148	1366.7707	0.0083
340.5057	0.0162	1475.9623	0.0096
355.6445	0.0175	1593.5531	0.0073
371.6401	0.0181	1720.7943	0.0063
388.4926	0.0185	1858.0432	0.0059
405.9164	0.0184		
424.1971	0.0176		
443.3347	0.0169		
463.3292	0.0169		
484.1807	0.0173		
505.8890	0.0172		
528.7399	0.0163		
552.4477	0.0152		
577.2980	0.0141		
603.2909	0.0121		
630.4263	0.0090		
658.9899	0.0058		
688.4104	0.0031		
719.5447	0.0010		
751.8216	0.0000		

Green River Shale	
Kerogen	
Pore Width (Å)	dV/dlog(W) Pore Volume (cm^3/g)
785.8123	0.0000
821.2311	0.0000
858.0782	0.0012
896.6390	0.0095
937.1993	0.0272
979.1878	0.0692
1000.0393	0.1603

Table A.7: Pore size distribution data for Green River kerogen and bulk shale CO_2 and N_2 gas adsorption.

	CO2 Data
	N2 Data

Woodford Shale			
Kerogen		Bulk Shale	
Pore Width (Å)	dV/dlog(W) Pore Volume (cm^3/g)	Pore Width (Å)	dV/dlog(W) Pore Volume (cm^3/g)
4.0181	0.0000	4.1928	0.0000
4.1928	0.0000	4.3675	0.0004
4.3675	0.0004	4.5422	0.0011
4.5422	0.0023	4.7169	0.0017
4.7169	0.0041	4.8916	0.0015
4.8916	0.0047	5.0663	0.0010
5.0663	0.0043	5.2410	0.0012
5.2410	0.0045	5.4157	0.0024
5.4157	0.0062	5.5904	0.0037
5.5904	0.0088	5.7651	0.0041
5.7651	0.0105	5.9398	0.0035
5.9398	0.0107	6.1145	0.0027
6.1145	0.0095	6.2892	0.0022
6.2892	0.0075	6.4639	0.0020
6.4639	0.0053	6.6386	0.0018
6.6386	0.0036	6.8133	0.0013
6.8133	0.0027	6.9880	0.0010
6.9880	0.0028	7.1627	0.0012
7.1627	0.0036	7.3374	0.0022
7.3374	0.0044	7.5121	0.0029
7.5121	0.0047	7.6868	0.0020
7.6868	0.0043	7.8615	0.0008
7.8615	0.0050	8.0362	0.0018
8.0362	0.0092	8.5781	0.0000
10.9013	0.0000	9.2929	0.0000
11.7948	0.0000	10.0077	0.0000
12.6884	0.0014	10.9013	0.0000
13.5819	0.0051	11.7948	0.0000
14.8329	0.0110	12.6884	0.0002
15.9052	0.0187	13.5819	0.0007
17.1561	0.0225	14.8329	0.0013
18.5858	0.0258	15.9052	0.0015
20.0155	0.0269	17.1561	0.0010

Woodford Shale			
Kerogen		Bulk Shale	
Pore Width (Å)	dV/dlog(W) Pore Volume (cm^3/g)	Pore Width (Å)	dV/dlog(W) Pore Volume (cm^3/g)
21.6239	0.0254	18.5858	0.0004
23.4110	0.0253	20.0155	0.0000
25.1980	0.0245	21.6239	0.0000
27.3426	0.0246	23.4110	0.0000
29.4871	0.0260	25.1980	0.0000
31.8103	0.0263	27.3426	0.0000
34.3122	0.0266	29.4871	0.0000
36.9929	0.0262	31.8103	0.0000
40.0309	0.0268	34.3122	0.0001
43.2477	0.0292	36.9929	0.0001
46.6432	0.0317	40.0309	0.0001
50.3961	0.0345	43.2477	0.0001
54.3277	0.0363	46.6432	0.0003
58.7954	0.0375	50.3961	0.0005
63.4419	0.0387	54.3277	0.0007
68.4458	0.0381	58.7954	0.0009
73.9858	0.0385	63.4419	0.0012
79.8832	0.0414	68.4458	0.0015
86.3167	0.0461	73.9858	0.0017
93.1077	0.0487	79.8832	0.0019
100.6135	0.0480	86.3167	0.0025
108.6554	0.0482	93.1077	0.0027
117.2335	0.0495	100.6135	0.0027
126.5264	0.0513	108.6554	0.0027
136.7128	0.0540	117.2335	0.0028
147.6141	0.0578	126.5264	0.0034
159.4089	0.0616	136.7128	0.0038
172.0973	0.0647	147.6141	0.0039
185.8579	0.0673	159.4089	0.0038
200.6908	0.0719	172.0973	0.0042
216.5960	0.0780	185.8579	0.0050
233.9308	0.0820	200.6908	0.0050
252.5166	0.0845	216.5960	0.0051
272.7108	0.0824	233.9308	0.0059

Woodford Shale			
Kerogen		Bulk Shale	
Pore Width (Å)	dV/dlog(W) Pore Volume (cm³/g)	Pore Width (Å)	dV/dlog(W) Pore Volume (cm³/g)
294.5134	0.0696	252.5166	0.0063
317.9243	0.0761	272.7108	0.0061
343.3011	0.1030	294.5134	0.0045
370.6436	0.1132	317.9243	0.0051
400.3094	0.1081	343.3011	0.0076
432.2984	0.0831	370.6436	0.0081
466.7894	0.0787	400.3094	0.0081
503.9609	0.1001	432.2984	0.0060
544.1706	0.1124	466.7894	0.0058
587.5970	0.0943	503.9609	0.0072
634.4189	0.0874	544.1706	0.0069
684.9937	0.0892	587.5970	0.0059
739.6788	0.0592	634.4189	0.0076
798.6530	0.0607	684.9937	0.0121
862.4523	0.0956	739.6788	0.0087
931.2554	0.1191	798.6530	0.0080
1005.5987	0.1068	862.4523	0.0097
1085.6605	0.1231	931.2554	0.0087
1172.3347	0.1681	1005.5987	0.0060
1265.7998	0.1201	1085.6605	0.0054
1366.7707	0.1096	1172.3347	0.0051
1475.9623	0.1339		
1593.5531	0.0941		
1720.7943	0.0853		

Table A.8: Pore size distribution data for Woodford kerogen and bulk shale CO_2 and N_2 gas adsorption.

	CO2 Data
	N2 Data

Cameo Coal	
Pore Width (Å)	dV/dlog(W) Pore Volume (cm^3/g)
18.5858	0.0018
20.0155	0.0004
21.6239	0.0000
23.4110	0.0007
25.1980	0.0021
27.3426	0.0035
29.4871	0.0046
31.8103	0.0052
34.3122	0.0055
36.9929	0.0056
40.0309	0.0062
43.2477	0.0075
46.6432	0.0089
50.3961	0.0101
54.3277	0.0108
58.7954	0.0112
63.4419	0.0116
68.4458	0.0112
73.9858	0.0105
79.8832	0.0108
86.3167	0.0122
93.1077	0.0124
100.6135	0.0109
108.6554	0.0101
117.2335	0.0099
126.5264	0.0101
136.7128	0.0103
147.6141	0.0101
159.4089	0.0097
172.0973	0.0098
185.8579	0.0101
200.6908	0.0097
216.5960	0.0096
233.9308	0.0100
252.5166	0.0101

Cameo Coal	
Pore Width (Å)	dV/dlog(W) Pore Volume (cm^3/g)
272.7108	0.0094
294.5134	0.0072
317.9243	0.0075
343.3011	0.0099
370.6436	0.0099
400.3094	0.0094
432.2984	0.0068
466.7894	0.0063
503.9609	0.0081
544.1706	0.0087
587.5970	0.0069
634.4189	0.0072
684.9937	0.0096
739.6788	0.0071
798.6530	0.0069
862.4523	0.0089
931.2554	0.0085
1005.5987	0.0062
1085.6605	0.0059
1172.3347	0.0076
1265.7998	0.0051
1366.7707	0.0045
1475.9623	0.0052
1593.5531	0.0036
1720.7943	0.0031
1858.0432	0.0035
2006.1934	0.0022
2166.3171	0.0018
2339.1294	0.0014
2525.7022	0.0018

Table A.9: Pore size distribution data for Cameo Coal CO_2 and N_2 gas adsorption.

	CO2 Data
	N2 Data

REFERENCES

Adesida, A.G. et al., 2011. SPE 147397 Kerogen Pore Size Distribution of Barnett Shale using DFT Analysis and Monte Carlo Simulations. *SPE Annual Technical Conference and Exhibition*, pp.1–14.

Chalmers, G.R., Bustin, M.R. & Power, I.M., 2012. Characterization of gas shale pore systems by porosimetry, pycnometry, surface area, and field emission scanning electron microscopy/transmission electron microscopy image analyses: Examples from the Barnett, Woodford, Haynesville, Marcellus, and Doig uni. *AAPG Bulletin*, 96(6), pp.1099–1119. Available at: http://search.datapages.com/data/doi/10.1306/10171111052 [Accessed January 10, 2015].

Lastoskie, C., Gubbins, K.E. & Quirke, N., 1993. Pore size distribution analysis of microporous carbons: A density functional theory approach. *Journal of Physical Chemistry*, 97(18), pp.4786–4796. Available at: http://www.scopus.com/inward/record.url?eid=2-s2.0-0012204736&partnerID=40&md5=7ee8d0114c4517ad33f5e1a0c68d411f.

Liu, H. & Seaton, N.A., 1994. Determination of the connectivity of porous solids from nitrogen sorption measurements—III. Solids containing large mesopores. *Chemical Engineering Science*, 49(11), pp.1869–1878.

Liu, Q.-S. et al., 2010. Adsorption isotherm, kinetic and mechanism studies of some substituted phenols on activated carbon fibers. *Chemical Engineering Journal*, 157(2-3), pp.348–356.

McCarthy, K. et al., 2011. Basic Petroleum Geochemistry for Source Rock Evaluation. *Oilfield Review*, 23, pp.32–43. Available at: http://www.slb.com/~/media/Files/resources/oilfield_review/ors11/sum11/basic_petroleum.pdf.

Milliken, K.L. et al., 2013. Organic matter-hosted pore system, Marcellus Formation (Devonian), Pennsylvania. *AAPG Bulletin*, 97, pp.177–200.

Ryu, Z. et al., 1999. Characterization of pore size distributions on carbonaceous adsorbents by DFT. *Carbon*, 37(8), pp.1257–1264. Available at: http://cat.inist.fr/?aModele=afficheN&cpsidt=1876595 [Accessed April 20, 2015].

Sangwichien, C., Aranovich, G.. & Donohue, M.., 2002. Density functional theory predictions of adsorption isotherms with hysteresis loops. *Colloids and Surfaces A: Physicochemical and Engineering Aspects*, 206(1-3), pp.313–320.

Shabro, V., Torres-Verdin, C. & Sepehrnoori, K., 2012. Forecasting Gas Production in Organic Shale with the Combined Numerical Simulation of Gas Diffusion in Kerogen, Langmuir Desorption from Kerogen Surfaces, and Advection in Nanopores. *Proceedings of SPE Annual Technical Conference and Exhibition*, p.SPE 159250. Available at: http://www.onepetro.org/mslib/servlet/onepetropreview?id=SPE-159250-MS&soc=SPE.

Sing, K., 2001. The use of nitrogen adsorption for the characterisation of porous materials. *Colloids and Surfaces A: Physicochemical and Engineering Aspects*, 187-188, pp.3–9. Available at: http://www.sciencedirect.com/science/article/B6TFR-43C5254-2/2/fdfe980f7a5f9e35dfcbb0fb2549a83a.

Singh, Harpreet, Farzam Javadpour, Amin Ettehadtavakkol, and Hamed Darabi. 2014. 'Nonempirical Apparent Permeability Of Shale'. *SPE Reservoir Evaluation & Engineering* 17 (03): 414-424. doi:10.2118/170243-pa.

Steele, W.A., 1973. The Physical Interaction of Gases with Crystalline Solids. *North-Holland Publishing Co.*, 36, pp.317–352.

Thommes, M. (Dr) & Quantachrome Instruments, 2003. Pore Size Analysis by Gas Adsorption Part I: Aspects of the Application of Density Functional Theory (DFT) and Monte Carlo simulation (MC) for micro/mesopore size analysis. *Powder Tech Note 31*, 9888(Mc), pp.1–7.

Wong, Y.C. et al., 2004. Adsorption of acid dyes on chitosan - Equilibrium isotherm analyses. *Process Biochemistry*, 39(6), pp.693–702.

Zhang, T. et al., 2012. Effect of organic-matter type and thermal maturity on methane adsorption in shale-gas systems. *Organic Geochemistry*, 47, pp.120–131.